Volume 17, Issue 2, 172513 (1-21)

Iranian Journal of Earth Science (IJES)

https://doi.org/10.57647/j.ijes.2025.1702.13

Geochemistry and Tectono-magmatic setting of Eshkavarat A_1-type granitoid in Southern Caspian Sea: Derived from underplated rocks related to oceanic Plume in Northern Iran

Milad Rezania ye Komachaly, Mojgan Salavati*, Saeid Hakimi Asiabar

Department of Geology, Lahijan Branch, Islamic Azad University, Lahijan, Iran.

***Corresponding author:** salavati1973@gmail.com

Original Research

Received:
28 March 2024
Revised:
6 June 2024
Accepted:
17 October 2024
Published online:
10 April 2025

Abstract:

The Eshkavarat intrusive bodies, consisting of monzonite, quartz monzonite and syenite to granite composition, with late Cretaceous age, are located east of Gilan province in western Alborz and formed as 4 large bodies, in the southern part of the study area. Petrographically they show perthitic and micrographic textures and are composed of K-feldspar, quartz, plagioclase and biotite as main minerals with accessory iron oxides and apatite. These rocks have high SiO_2, alkalis, $FeO_{(total)}$/MgO. In the spider diagram show subparallel, linear, and homogeneous REE profiles with enrichment of LILE. Granitoid show high Ga/Al, Zr, Th, Rb, and rare earth elements (REE) (except Eu), low CaO, MgO and strong depletion in Ba, Eu and Sr. They have the typical geochemical characteristics of A_1-type granites. Tectonic discrimination diagrams show the tectonic setting of the within-plate granite (WPG). According to the tectonic model presented for the study area, a tectonic window and an extensional regime above the supra-subduction zone appear to have been created by the subduction of the oceanic crust of the southern Caspian Sea after the end of the Upper Cretaceous. The mantle magma then rose up through the tectonic window. Direct release of this mantle magma has generated oceanic plume-like (OIB) rocks in the region. This mantle magma, arrest under the crust, causing its partial melting, and finally, fractionational crystalisation of mafic minerals and minor crustal assimilation, primarily parent magma of A_1 granitoids and syenitic A_1 rocks was generated, then, by fractionation felsic minerals A_1-type granitic magmas were created.

Keywords: A-type granite; Oceanic plume; Southern Caspian Sea; Gilan; Iran

1. Introduction

Different types of magmatism can be found in the states of large igneous rocks (Kalantari et al., 2008; Ernst, 2014; Hari et al., 2018). These states can contain large amounts of alkaline volcanic rocks that are associated with non-orogenic granitoid rocks known as A-type granites (Zhu et al., 2010; Zhang and Zou, 2013). In Iran, granites of the I-, S-, and A-types occur in a wide variety. Recently, there have been several reports (Alirezaei and Hassanzadeh, 2012; Shafaii Moghadam et al., 2015; Ghaffari et al., 2015; Azizi et al., 2017; Honarmand et al., 2017; Mollai et al., 2021; Nazari et al., 2023) of A-type granites in different parts of Alborz, which are generally the result of post-collisional extensional activity. So far, different reasons have been proposed for the origin of Tertiary magmatism in Iran, so in some cases, the Neotethyan subduction zones and the collision of the Iranian and Arabian plates have been considered as the cause (Berberian and King, 1981; Moine-Vaziri, 1985), and in other cases it has been associated with intercontinental rifting (Sabzehei, 1974).

Recent studies of Tertiary magmatism in Alborz indicate that it is related to continental arc magmatism (Valizadeh et al., 2008), subduction zone magmatism in an active continental margin (Kalantari et al., 2008), and back-arc basin (BAB) subduction regime and magmatism (Asiabanha and Foden, 2012; Dabiri et al., 2018; Yazdi et al., 2021; Ousta

et al., 2024; Salehpour et al., 2025). Several felsic igneous rocks of different age and composition are exposed in the Gilan province of northern Iran. Within the pillow lavas of the South Caspian Ophiolite Complex (Late Cretaceous), Eshkavarat granitoid bodies of relative post-Cretaceous (Eocene?) age are exposed. Intrusive bodies younger than the Upper Cretaceous have been injected into the ophiolitic complex south of the Caspian Sea. As a result, numerous outcrops of granitoid bodies (monzonite to granitic) have been injected in the southern parts of the city of Amlesh and the Eshkavarat. Petrological and geochemical characteristics and the relationship between these bodies and the geotectonic of their genesis have not been studied, therefore this paper has attempted to study the petrology and geochemistry of the Eshkavarat granitoid bodies based on geochemical data as part of the Alborz-Azerbaijan Tertiary magmatism from the viewpoint of genesis and tectono-magmatic setting.

2. Study methods

For this study, fieldwork was carried out on the Eshkavarat granitoid bodies using 1:100,000 Javaherdeh and 1:2,500,000 Qazvin-Rasht maps. Due to the climatic conditions of the region, sudden rains and inadequate communication routes, the site was visited in 5 stages for a total of 10 days during the summers of 2020 and 2021. At the end of the fieldwork, 60 rock samples were taken for petrographic study based on field relations. 24 of the best-preserved samples were selected and analysed for whole-rock major and REE and other trace element concentrations following petrographic studies. The rock powders were first fused to ensure dissolution of all phases and then dissolved in hot HF and HNO_3 to prepare solutions from which trace element abundances were determined using Inductively Coupled Plasma Mass Spectrometry (ICP-MS) at the SGS (Société Générale de Surveillance) Analytical Laboratories in Canada. IGPET and GCDKIT software were then used to generate the necessary diagrams. Data were interpreted and analysed (Table 1).

3. Geology of the study area

The main granitoid studied, occurs as an elevated lensoidal body with a northeast-southwest trend, with 50°, 05′ 13″ east longitude and 36°, 55′ 18″ north latitude situation, and some smaller bodies, intruding the Upper Cretaceous assemblages and the upper parts of the southern Caspian Sea ophiolite sequences (Fig. 1), and is located 22 km southeast of Amlash city and east of Gilan province. The study area is located north of the Alborz fault and is part of the Alborz subsidence of the Caspian Sea (Aghanabati, 2006)) (Fig. 2). The study area is part of the Javaherdeh 1:100,000 geological map (Baharfiruzi and Shafeii, 2003) (Fig. 2). The dominant rocks of the area are well-preserved rocks of a Late Cretaceous ophiolite sequence (named the Southern Caspian Ophiolite (SCO) sequence by Salavati et al. (2013) and Salavati et al. (2008). Most of the study area is covered by pillow lavas and upper pelagic limestones of the upper part of this ophiolite sequence Salavati et al. (2008). Eshkavarat intrusive bodies have been injected into the pillow lavas and limestones (Fig. 1). All of these bodies show sharp contact with their host rocks.

Based on field and petrographic characteristics, the granitoid rocks exposed in the Eshkavarat area can be divided into three subgroups: granite, monzonite and syenite. The granites show intergranular, graphic, porphyritic and perthitic textures in microscopic studies (Fig. 3) and are composed mainly of K-feldspar, quartz and plagioclase with minor biotite and muscovite. Sphene and iron oxides are common accessory minerals, while sericite, kaolinite, epidote and chlorite are alteration minerals. Alkaline feldspars with a grain size of 4 to 8 mm account for about 65 vol%. Graphitic and perthitic textures due to intergrowths between quartz and alkali feldspar are common (Fig. 3 a and b). Plagioclase is euhedral to subhedral with 10 vol.% that sometimes has zoning. subhedral to anhedral quarz is $20-25$ vol.% (Fig. 3 a).

Monzonite type rocks are represented by monzo-syenite, monzonite and quartz monzonite. The microscopic picture shows granular, porphyritic and porphyritic microlite texture and rarely poikilitic texture with phenocrysts of K-feldspar and plagioclase (Fig. 4 a, b). The dominant mineral is plagioclase (40% by volume), sometimes with zoning. Euhedral K-feldspar (40 vol%) such as plagioclase, quartz (20 vol% in the quartz monzonite) and phenocrysts of clinopyroxene (10 vol%) with 2.5 mm size and minor biotite (15 vol%) with $1.5-2.5$ mm size, commonly altered to chlorite and iron oxides. A poikilitic texture (Fig. 4 c) was formed by feldspars surrounded by green Na-clinopyroxene. Thin sections show a variety of textures including granular, porphyritic, glomero-porphyritic and graphitic (Fig. 4 d, e and f). The main mineral assemblages consist of plagioclase, K-feldspar, and Na-clinopyroxene and accessory minerals are biotite and quartz. Sericite, kaolinite and chlorite are alteration minerals. Anhedral to subhedral perthitic K-feldspar with grain sizes of $0.2-2$ mm and $20-65$ Vol % is the dominant mineral. Alkali feldspars are sometimes mainly kaolinitic. Plagioclase and biotite are chloritised to some extent. Rarely, apatite and zircon are also present. The matrix consists of fine-grained quartz and plagioclase and K-feldspar microlite.

4. Geochemistry

The analysed samples are characterised by SiO_2: 51.2 to 72.8 wt%, TiO_2: 0.02 to 0.98 wt%, with Al_2O_3, CaO, and MgO respectively 11.98 to 20.00 wt%, 0.08 to 3.16 wt% and 0.05 to 1.61 wt%, alkali content (Na_2O: 3.22 to 9.6 wt% and K_2O: 2.41 to 6.16 wt%) and Fe_2O_3tot: 2.43 to 6.53 wt%. On the rock classification diagrams, SiO_2 versus total alkalis (K_2O+Na_2O), (De La Roche et al., 1980; Middlemost, 1985), (Fig. 5) and (Cox et al., 1979) the rocks studied fall into the of nepheline syenite, syenite, quartz-monzonite, and granite field (Fig. 5).

On the Harker diagrams, Al_2O_3, CaO, Fe_2O_3t, MgO, TiO_2, MnO, Zr, Ni and Sr decrease with SiO_2, whereas Rb, Ba are not significantly correlated with SiO_2 (Fig. 6), reflecting the fractionation of ferromagnesian minerals like hornblende, pyroxene and biotite.

Table 1. Major and trace element data of studied granitoeid samples by ICP-AES and ICP-MS Major and elements are given in wt% and ppm, respectively. Fe_2O_3 represents total iron oxide as ferric iron, LOI = Lost on ignition, AI (Agpatic Index: $(Na_2O+K_2O)/Al_2O_3$), ASI (Aluminium Saturation Index) = Al/(Ca-1.67P+Na+K), Fe-Index = $(FeO+0.9Fe_2O_3)/(FeO+0.9Fe_2O_3+MgO)$, MALI = (Modified alkali lime index: Na_2O+K_2O+CaO).

Rock type	Syenite	Granite-alkali granite	Syenite	Syenite	Granite-alkali granite	Granite-alkali granite	Monzonite-Q monzonite	Monzonite-Q monzonite	Granite-alkali granite	Monzonite-Q monzonite	Monzonite-Q monzonite	Monzonite-Q monzonite
sample No	KFS 700	KFS 6-2	KFS 600	KFS 800	KFS 500	KFS 550	KFS 400	KFS 450	KFS 4	KFS 3-1	KFS 3-2	KFS 1-2
SiO_2	51.2	69.8	60.8	60.7	72.1	70.2	57.80	58.00	68.4	55.30	55.20	61.30
TiO_2	0.04	0.32	0.28	0.27	0.29	0.30	0.98	0.98	0.35	0.94	0.93	0.92
Al_2O_3	20.0	12.3	17.0	17.0	12.1	11.98	15.30	15.10	14.6	14.70	14.70	14.90
Fe_2O_3	4.80	4.29	5.15	5.14	2.43	2.44	6.53	6.54	3.84	6.44	6.43	6.11
MnO	0.22	0.08	0.10	0.10	0.32	0.33	0.15	0.15	0.05	0.22	0.22	0.07
MgO	1.27	0.14	0.72	0.71	0.05	0.05	0.80	0.80	0.07	1.61	1.60	0.44
CaO	1.00	0.46	1.04	1.02	0.08	0.08	2.49	2.50	0.30	3.16	3.15	0.56
Na_2O	9.00	3.90	6.60	6.40	5.00	4.89	4.10	4.20	3.90	4.10	4.20	3.50
K_2O	2.41	4.61	2.98	2.99	2.97	2.90	4.73	4.63	5.69	4.07	4.06	5.86
P_2O_5	0.04	0.02	0.13	0.13	0.02	0.02	0.30	0.30	0.05	0.26	0.25	0.29
LOI	8.12	3.13	4.18	4.95	3.94	4.5	4.95	4.6	2.24	6.47	6.46	5.08
Sum	98.1	99.05	98.98	99.41	99.3	97.69	98.132	97.8	99.49	97.27	97.2	99.03
Ba	30	60	210	208	50	49	800	790	350	840	842	1490
Sr	260	30	110	112	30	32	270	272	180	300	300	200
Zn	143	62	91	90	35	36	115	114	95	167	166	107
Ag	0.99	0.99	0.99	0.99	0.99	0.99	0.99	0.99	0.99	0.99	0.99	0.99
Ce	260	159	147	148	183	181	112	111	156	129	128	94.9
Co	0.90	0.90	1.00	1.00	0.50	0.50	4.20	4.20	1.30	5.20	5.10	4.80
Cs	4.00	1.00	0.10	0.10	0.10	0.10	1.90	1.80	1.40	0.70	0.70	0.30
Cu	10.0	12.0	31.0	30.0	12.0	12.0	20.00	20.00	10.0	11.00	11.00	11.00
Dy	6.17	8.24	5.25	5.20	10.7	10.8	7.38	7.39	7.15	7.74	7.73	7.60
Er	3.87	4.23	3.29	3.20	5.88	5.99	3.95	3.94	4.39	3.91	3.90	4.16
Eu	1.39	0.93	1.61	1.60	0.85	0.90	3.52	3.52	1.20	3.67	3.66	3.25
Ga	34.0	30.0	29.0	28.0	32.0	32.0	29.00	28.50	33.0	29.00	28.00	24.00
Gd	6.76	10.4	5.67	5.66	11.4	11.4	9.18	9.17	7.04	9.77	9.76	9.07
Hf	15.0	15.0	17.0	17.0	18.0	17.0	11.00	11.00	15.0	11.00	11.00	11.00
Ho	1.18	1.55	1.05	1.04	2.05	2.04	1.41	1.40	1.45	1.37	1.35	1.44
La	178	86.1	90.5	90.4	96.6	96.5	61.40	61.50	60.5	72.30	72.20	59.50
Lu	0.52	0.62	0.59	0.58	0.82	0.82	0.48	0.49	0.66	0.44	0.44	0.56
Mo	2.00	3.00	2.00	2.00	5.00	5.00	6.00	6.00	6.00	4.00	4.00	2.00
Nb	146	117	103	103	141	140	82	82	116	78	78	83
Nd	69.8	68.5	48.6	48.6	69.9	69.6	52.30	52.20	46.2	58.30	58.20	49.60
Ni	5.00	6.00	5.00	5.00	5.00	5.00	5.00	5.00	5.00	5.00	5.00	6.00
Pr	24.8	18.6	15.2	15.1	19.3	19.2	13.7	13.6	13.0	15.4	15.3	13.0
Rb	85.3	158	42.2	42.15	98.1	98	107	107	191	103	103	90.10
Sm	9.90	13.9	8.10	5.20	14.8	18.7	11.20	11.20	9.20	12.30	12.30	11.00

Continued of Table 1

Rock type	Syenite	Granite-alkali granite	Syenite	Syenite	Granite-alkali granite	Granite-alkali granite	Monzonite-Q monzonite	Monzonite-Q monzonite	Granite-alkali granite	Monzonite-Q monzonite	Monzonite-Q monzonite	Monzonite-Q monzonite
sample No	KFS 700	KFS 6-2	KFS 600	KFS 800	KFS 500	KFS 550	KFS 400	KFS 450	KFS 4	KFS 3-1	KFS 3-2	KFS 1-2
Sn	7.00	7.00	7.00	7.00	8.00	8.00	5.00	5.00	5.00	4.00	4.00	6.00
Ta	13.2	8.20	7.70	7.70	9.50	9.60	5.40	5.50	8.50	5.10	5.10	5.60
Tb	1.07	1.63	0.91	0.91	1.90	1.80	1.41	1.42	1.22	1.45	1.44	1.40
Th	29.5	15.3	15.9	15.9	21.5	21.4	10.40	10.40	21.6	10.00	10.00	11.10
Tl	0.50	0.50	0.50	0.50	0.50	0.50	0.50	0.50	0.50	0.50	0.50	0.50
Tm	0.49	0.52	0.45	0.45	0.81	0.80	0.46	0.46	0.53	0.43	0.44	0.50
U	8.46	3.18	3.92	3.90	2.46	2.44	2.53	2.54	3.97	2.30	2.20	2.98
V	5.00	10.0	8.00	8.00	5.00	5.00	24.00	22.00	12.0	23.00	22.00	24.00
W	1.00	6.00	3.00	3.00	5.00	5.00	2.00	2.00	3.00	2.00	2.00	2.00
Y	36.6	37.7	32.4	32.4	52.9	52.7	40.80	40.80	38.9	39.70	39.70	41.30
Yb	3.60	4.00	3.70	3.70	5.30	5.20	3.40	3.40	4.20	3.20	3.20	3.70
Zr	806	581	935	934	728	725	461	460	562	435	433	456
$(Th/Nb)_N$	1.41	0.92	1.08	1.08	1.07	1.07	0.89	0.89	1.30	0.90	0.90	0.94
Fe Index	0.77	0.97	0.87	0.87	0.98	0.98	0.88	0.88	0.98	0.78	0.78	0.93
AL	1.37	-2.06	1.13	1.41	-1.09	-0.92	0.27	0.10	-1.73	0.82	0.69	-1.14
ASI	1.35	0.83	1.04	1.06	0.91	0.92	0.94	0.93	0.88	0.94	0.93	0.93
MALI	12.41	8.97	10.62	10.41	8.05	7.87	11.32	11.33	9.89	11.33	11.41	9.92
$(Th/Ta)^*_N$	1.36	1.14	1.26	1.26	1.38	1.36	1.17	1.15	1.55	1.20	1.20	1.21
$(Th/Nb)^*_N$	0.07	0.05	0.06	0.06	0.06	0.06	0.05	0.05	0.07	0.05	0.05	0.05
$(Rb/Sr)^*_N$	0.19	3.03	0.22	0.22	1.88	1.76	0.23	0.23	0.61	0.20	0.20	0.26
SiO_2	61.10	68.10	60.00	67.90	59.20	70.40	72.80	73.00	71.50	57.50	57.40	58.20
TiO_2	0.91	0.33	0.05	0.27	0.05	0.35	0.31	0.32	0.34	0.02	0.14	0.15
Al_2O_3	14.80	13.70	18.50	15.00	18.95	13.57	13.50	13.40	13.55	19.05	18.65	18.75
Fe_2O_3	6.10	3.68	3.03	4.83	4.59	3.89	3.76	3.86	3.85	4.25	5.70	5.80
MnO	0.06	0.05	0.17	0.09	0.18	0.07	0.08	0.08	0.08	0.22	0.05	0.05
MgO	0.48	0.06	0.05	0.13	0.00	0.14	0.09	0.09	0.09	0.02	0.28	0.29
CaO	0.59	0.20	0.68	0.28	0.74	0.75	0.18	0.19	0.18	0.86	1.98	1.88
Na_2O	3.55	3.40	9.60	7.03	9.34	3.22	4.50	4.60	4.30	9.46	5.36	5.26
K_2O	5.83	6.16	5.40	2.69	4.91	6.01	4.18	4.19	5.19	4.87	5.98	5.88
P_2O_5	0.29	0.05	0.03	0.01	0.00	0.02	0.02	0.02	0.02	0.06	0.07	0.07
LOI	5.5	3.02	2.03	1.85	2.81	2.27	1.06	1.02	1.3	3.12	3.61	3.6
Sum	99.21	98.75	99.54	100.08	100.77	100.96	100.84	100.77	100.4	99.43	99.22	99.93
Ba	1491	420.0	15.00	21.90	2.90	636.0	588.0	630.0	590.0	3.70	16.90	16.80
Sr	201.0	160.0	9.00	28.80	22.30	88.70	22.50	88.70	22.10	5.40	60.90	61.00
Zn	106.0	65.00	1.50	150.0	158.0	93.00	132.0	92.00	131.0	188.0	125.0	124.0
Ag	0.99	0.99	0.99	0.99	0.99	0.99	0.99	0.99	0.99	0.99	0.99	0.99
Ce	94.30	154.0	200.0	457.0	233.0	150.0	186.0	151.0	185.0	372.0	266.0	265.0
Co	4.70	1.10	1.00	2.20	0.80	1.30	0.60	1.20	0.50	0.90	2.00	2.00

Continued of Table 1

Rock type	Syenite	Granite-alkali granite	Syenite	Syenite	Syenite	Granite-alkali granite	Granite-alkali granite	Granite-alkali granite	Granite-alkali granite	Syenite	Syenite	Syenite
sample No	KFS 1-3	KFS 103	SB70	118	A91	Kh1	Kh2	Kh3	Kh4	R113	R116-1	R112
Cs	0.30	0.90	1.12	0.09	1.98	1.19	0.84	1.18	0.85	4.63	0.71	0.70
Cu	11.00	11.00	10.00	12.00	5.00	4.00	6.00	5.00	6.00	7.00	5.00	5.00
Dy	7.40	8.26	10.60	18.15	11.55	9.39	11.75	9.38	11.74	12.75	10.10	10.20
Er	4.13	4.32	6.50	10.65	7.40	4.80	6.19	4.70	6.15	7.95	5.58	5.59
Eu	3.22	1.44	0.95	1.11	1.07	1.75	1.25	1.74	1.24	1.08	1.28	1.29
Ga	24.00	26.00	24.00	41.20	41.90	24.40	31.00	24.00	31.00	37.80	29.20	29.10
Gd	9.06	9.60	9.70	23.90	12.25	11.45	14.15	11.40	14.17	16.30	14.35	14.55
Hf	11.00	15.00	14.00	24.10	26.30	13.40	17.60	13.30	17.50	26.30	16.00	16.00
Ho	1.43	1.54	1.55	3.43	2.32	1.62	2.03	1.61	2.02	2.48	1.80	1.90
La	59.40	77.70	128.0	246.0	134.0	77.10	93.80	93.20	92.80	223.0	140.5	140.4
Lu	0.55	0.60	0.55	1.68	1.17	0.64	0.81	0.63	0.82	1.12	0.76	0.76
Mo	2.00	5.00	5.00	8.00	9.00	3.00	3.00	3.00	3.00	12.00	2.00	2.00
Nb	83.00	110.0	126.0	205.0	144.0	111.5	143.5	111.4	1434.	260.0	325.0	324.0
Nd	49.80	61.70	67.00	151.5	70.40	58.60	72.90	58.50	72.70	101.5	91.30	91.10
Ni	6.00	5.00	6.00	8.00	0.00	4.90	8.00	5.00	7.50	4.90	4.90	4.80
Pr	14.00	17.20	17.10	47.30	22.80	17.00	20.50	16.00	20.00	35.30	28.30	28.20
Rb	90.20	192.0	115.0	53.30	108.0	159.5	141.0	159.0	140.0	140.0	180.5	180.4
Sm	11.00	12.50	11.30	24.40	12.10	11.65	14.70	11.60	14.30	15.10	14.75	14.75
Sn	6.00	9.00	6.00	12.00	11.00	5.00	8.00	5.00	8.00	11.00	6.00	6.00
Ta	5.60	7.90	7.30	11.90	11.20	7.00	9.00	7.00	9.00	20.80	17.10	17.00
Tb	1.30	1.52	1.50	3.43	1.96	1.72	2.20	1.71	2.10	2.35	1.95	1.85
Th	11.20	20.10	22.80	35.00	28.00	18.55	24.50	18.45	24.30	44.80	24.50	24.40
Tl	0.50	0.50	0.50	0.40	0.40	0.40	0.40	0.40	0.40	0.40	0.40	0.40
Tm	0.50	0.56	0.50	1.51	1.08	0.66	0.81	0.65	0.80	1.14	0.73	0.73
U	2.96	3.88	3.01	2.54	8.60	3.52	2.05	3.51	2.03	12.10	5.78	5.88
V	23.00	10.00	3.00	12.00	4.90	4.90	4.90	4.90	4.90	4.90	4.90	4.70
W	2.00	3.00	2.00	9.00	5.00	5.00	24.00	5.00	23.00	7.00	17.00	17.00
Y	41.30	41.30	65.00	88.10	62.10	40.20	51.90	40.00	52.00	68.20	46.00	46.00
Yb	3.70	4.00	6.60	9.49	6.81	4.04	4.83	4.03	4.84	6.85	4.53	4.55
Zr	455	582	1300	1020	1320	502	688	500	680	1240	681	682
$(Th/Nb)_N$	0.94	1.28	1.27	1.20	1.36	1.16	1.20	1.16	0.12	1.21	0.53	0.53
Fe Index	0.92	0.98	0.98	0.97	1.00	0.96	0.97	0.97	0.97	0.99	0.95	0.95
AL	-1.26	-2.64	-6.02	-0.89	-4.38	-2.24	-1.09	-1.35	-2.46	-4.40	-0.58	-0.17
ASI	0.92	0.83	0.73	0.93	0.78	0.82	0.92	0.90	0.83	0.79	0.90	0.93
MALI	9.97	9.76	15.68	10.00	14.99	9.98	8.86	8.98	9.67	15.19	13.32	13.02
$(Th/Ta)^*_N$	1.22	1.55	1.90	1.79	1.52	1.62	1.66	1.61	1.65	1.31	0.87	0.88
$(Th/Nb)^*_N$	0.05	0.07	0.07	0.06	0.07	0.06	0.06	0.06	0.01	0.06	0.03	0.03
$(Rb/Sr)^*_N$	0.26	0.69	7.36	1.07	2.79	1.04	3.61	1.03	3.65	30.28	1.71	1.70

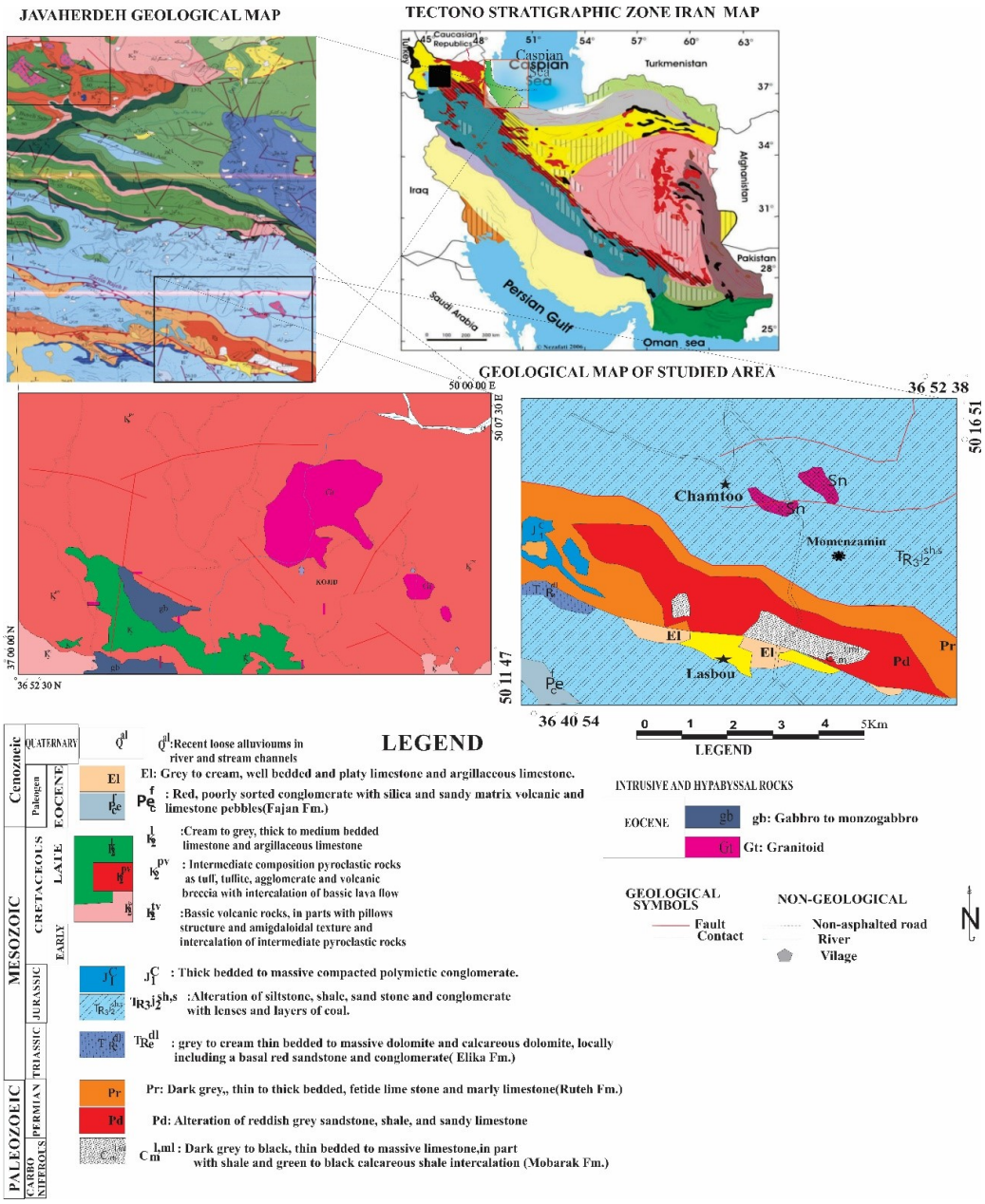

Figure 1. Geological map of the studied area in the Southern Caspian Sea (redraw based on Javaherdeh 1:100000 map (Baharfiruzi and Shafeii, 2003). Tectono-stratigraphic zones of Iran and location of study area ,(after Aghanabati (2006)).

On the classification diagrams based on the Fe-index of Frost et al. (2001), the studied samples are ferroan (Fig. 7 a). Similarly, the calculation of the modified alkalinity index (MALI = Na_2O+K_2O)-CaO) of the studied samples varies between 2.13 and 7.58 and is alkaline to alkaline calcic (Fig. 7 b). The values of the Alkalinity Index (AI = Al − (K + Na)) in the samples show that all the samples tend to be peralkaline rather than per- and meta-aluminous (Fig. 7 c). Spider diagrams normalised to MORB (Pearce, 1983) (Fig. 8 a) and primitive mantle (Sun and McDonough, 1989) (Fig. 8 c) show negative anomalies in Ba, P, Ti and Sr and positive anomalies in K, Th, Rb and U, similar to the pattern of post-collision granites (Pearce et al., 1984). The amount of Sr and Ba is more similar to post-orogenic calc-alkaline granites. On spider diagrams normalised to chondrites (Sun and McDonough, 1989) (Fig. 8 b), the studied samples have a specific enrichment of all REE between 10 and 110 times that of chondrites, and at the same time they show an enrichment of LREE to HREE. The trend of elements in all samples compared to chondrites (Fig. 8 b) is almost parallel and the samples are rich in LREE to HREE ($(La/Yb)_N$ = 9.6 − 32.96). Negative Ti anomalies and a decreasing trend correlation between TiO_2 and SiO_2, as well as relatively high concentrations of Nb and Ta in the Eshkavarat A_1-type granitoids, suggest the crystallisation of ilmenite and titanite, as titanite has a higher partition coefficient for Nb and Ta (Xiong et al., 2005; Bédard, 2006).

Separation of plagioclase, K-feldspar and apatite minerals during magmatic evolution may be indicated by negative Eu, Sr, Ba and P anomalies in the rocks studied. Ba can easily replace K in biotite and feldspar. This may be associated with the fractional crystallisation of feldspar at higher tempera-

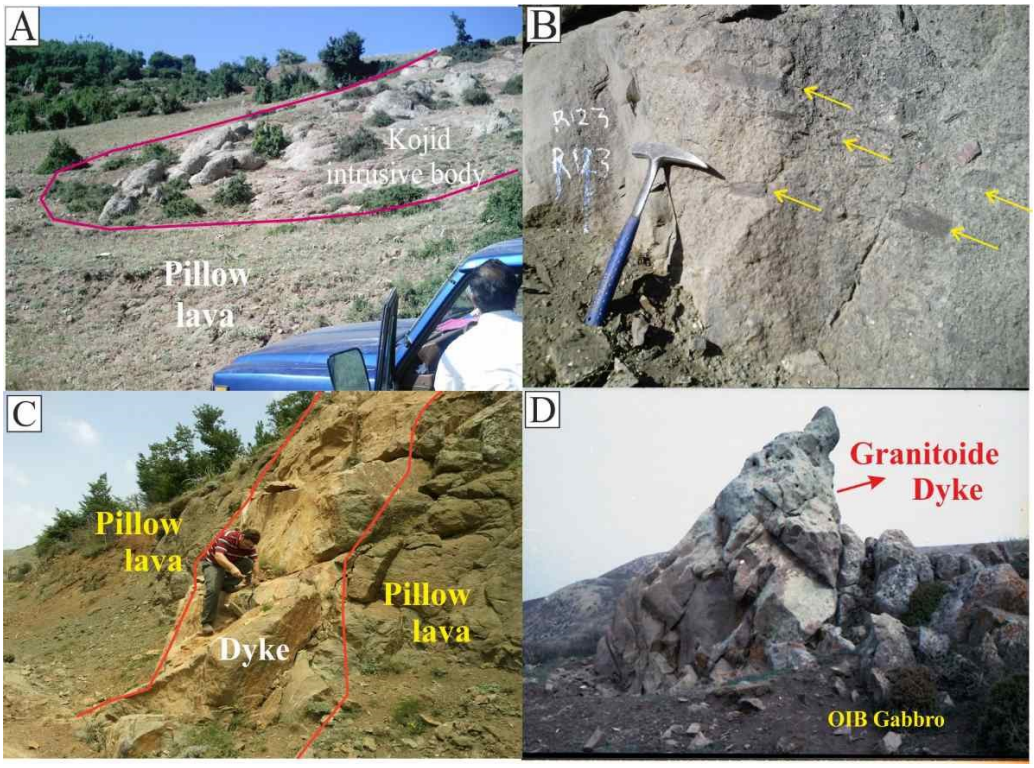

Figure 2. Field images of the Kojid granitoid rocks (A): contact between the Kojid intrusive rocks and pillow lavas of the southern Caspian Sea ophiolite sequence (looking northwest), (B): view of the chilled margin of the Kojid intrusive mass through the flow structure and with enclave rocks of the host basalts (yellow markers). (C), (D): Injected dikes from the Kojid dyke to OIB pillow lavas and gabbro.

tures than hornblende and biotite (Rollinson, 1993; Arslan and Aslan, 2006). Enrichment in LILE and HFSE elements with negative anomalies in Nb-Ti-Ta is a subduction-related magma characteristic, usually attributed either to a mantle source previously enriched in LILE and HFSE elements due to metasomatic activity of fluids derived from sediments or subducted plate (Pearce, 1983; Ilbeyli et al., 2004) or may characterise magmas derived from a subcontinental lithospheric mantle formed during early subduction. The relatively smooth distribution patterns of the HREE in the normalised diagram relative to the chondrite indicate that there is little differentiation in the HREE (Pearce, 1983). The depletion of Nb-Ti-Ta can be explained by the retention of titanium-rich residual mineral phases (such as rutile and titanite) at the mantle source (Foley and Wheller, 1990).

Based on the diagrams of different granitoids types, the studied samples with a high Ga/Al ratio indicate an A-type nature (Whalen et al., 1987) (Fig. 9). Also in the Zr + Nb + Ce + Y vs. FeO^*/MgO diagram, all samples are plotted in an A-type granite field (Fig. 9 d). For granitoids showing the A-type field in the diagrams of Whalen et al. (1987) and the WPG field in the diagram of Pearce et al. (1984) (Eby, 1992), discrimination diagrams are used which separate A_1-type granites from A_2-type granites.

As mentioned above, all samples plot within the A-type field in the diagrams of Whalen et al. (Whalen et al., 1987) (Fig. 9) and fall into the within-plate and post-orogenic granite field in the tectonic diagrams of Y + Nb and Y+Ta versus Rb; Y versus Nb and Yb versus Ta, (Fig. 10), also on the Rb-Ta-Hf and Rb-Nb-Hf diagrams (Harris et al., 1986) (Fig. 11), which include the four WPG, ORG, VAG and COLG fields, the studied rocks plot in WPG. The discrimination granitoid diagrams were used to separate the A_1 and A_2 types.

In these diagrams, all the samples are plotted in the A_1-type field (Fig. 12). Recent studies show that in the A_1-type granites, Th/Nb > 1.5, and in the A_2-type granites Th/Nb < 2 (Eby, 2011; Moreno et al., 2014). In the studied samples, 0.11 > Th/Nb > 1.4 so they have the characteristics of the A_1-type granite. nite.

5. Discussion

5.1 Petrogenesis of Eshkavarat A_1-type granites

All the geochemical and petrographic data show that the granitoids studied are typical A-type granites. On the diagrams of the different types of granitoids and their tectono-magmatic setting, almost all the studied granitoid rocks are plotted in WPG and are A_1-type granitoids. Th/Ta, Th/Nb and Rb/Sr ratios are used to determine the source of A-type granites due to their high sensitivity to mantle or crustal origin (Rudnick and Gao, 2003; Plank, 2005; Jiang et al., 2020). For granites of mantle origin, these ratios are $(Th/Ta)_N = 2.15$ and $(Th/Nb)_N = 0.12$ (normalised to pyrolite according to McDonough and Sun (1995)). The samples studied have $(Th/Ta)_N = 0.01 - 1.55$ and $(Th/Nb)_N = 0.01 - 0.07$. These values are similar to those of A-type granites of mantle origin. However, the ratio of $(Rb/Sr)_N = 63$ shows much higher values compared to mantle granites. This may be due to the influence of subduction parts and the tectonic setting of the studied granitoids.

The term A-type granite is used to describe granites that are

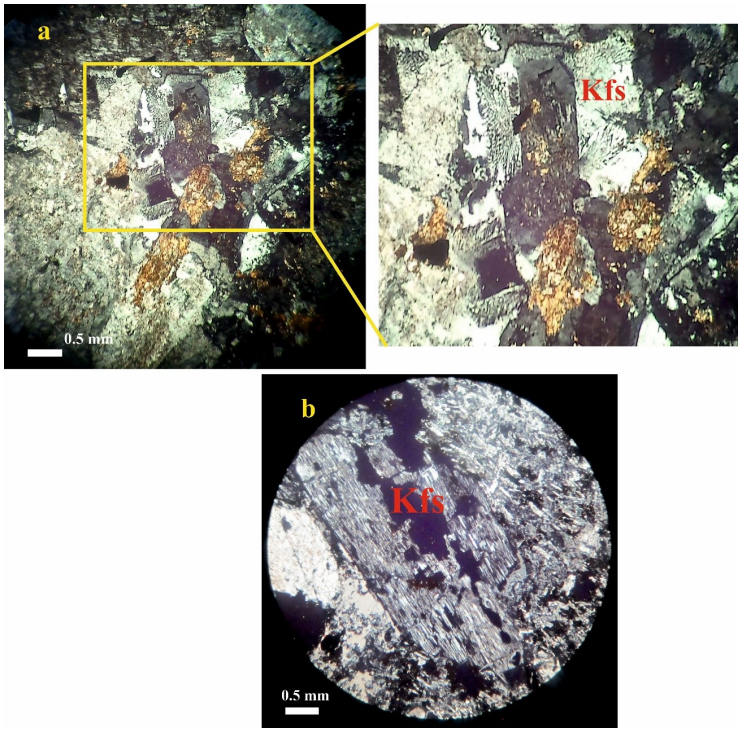

Figure 3. Photomicrographs of the Kojid granitoid (A): Micrographic texture, intergrowths between quartz and alkali feldspar (Kfs) are common, (B): larger perthitic alkali feldspar crystals (Kfs) and minor plagioclase.

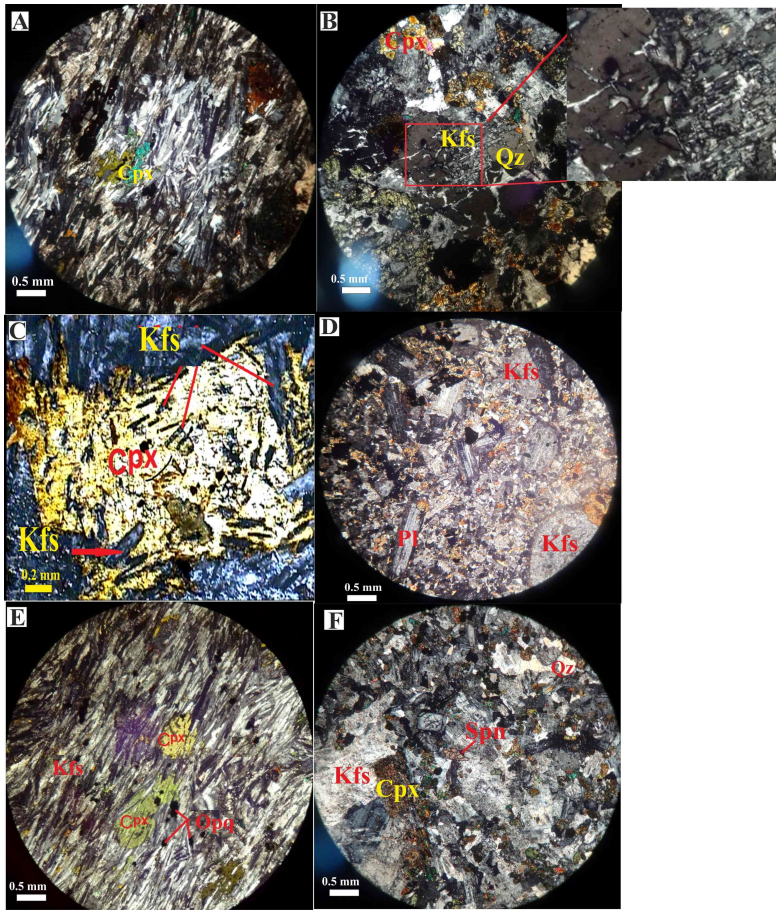

Figure 4. (A): Porphyritic microlite texture in monzonite, (B): Graphyitic and perthitic texture in quartz monzonite, (C): Porphyritic microlite texture in syenite, (D): Phenocryst of K-feldspar and plagioclase in syenite, (E): Poikilitic texture in Monzo-syenite, (F): granular texture in quartz syenite. (in crossed polarized light), Abbreviations after Whitney and Evans (2010) (Pl: Plagioclase, Kfs: alkali feldspar, Qz: Quartz, Opq: Opaque minerals, Spn: Sphene).

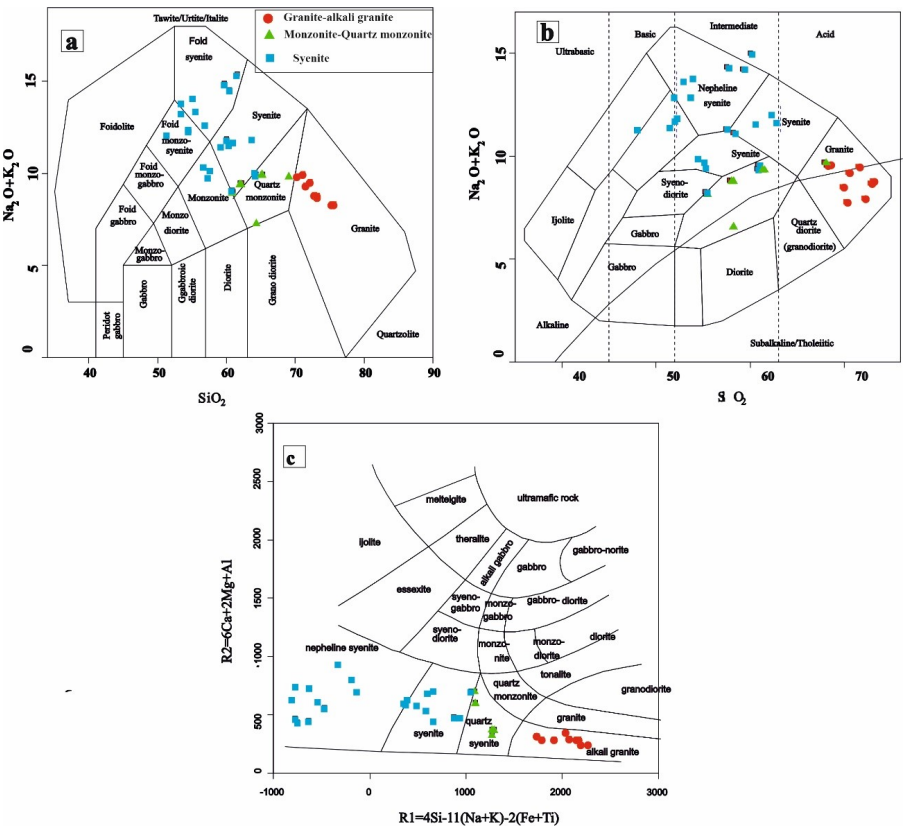

Figure 5. Plotting of samples from studied granitoid on diagrams of (A): after Middlemost (1985), (B): Cox et al. (1979), and (C): after De La Roche et al. (1980).

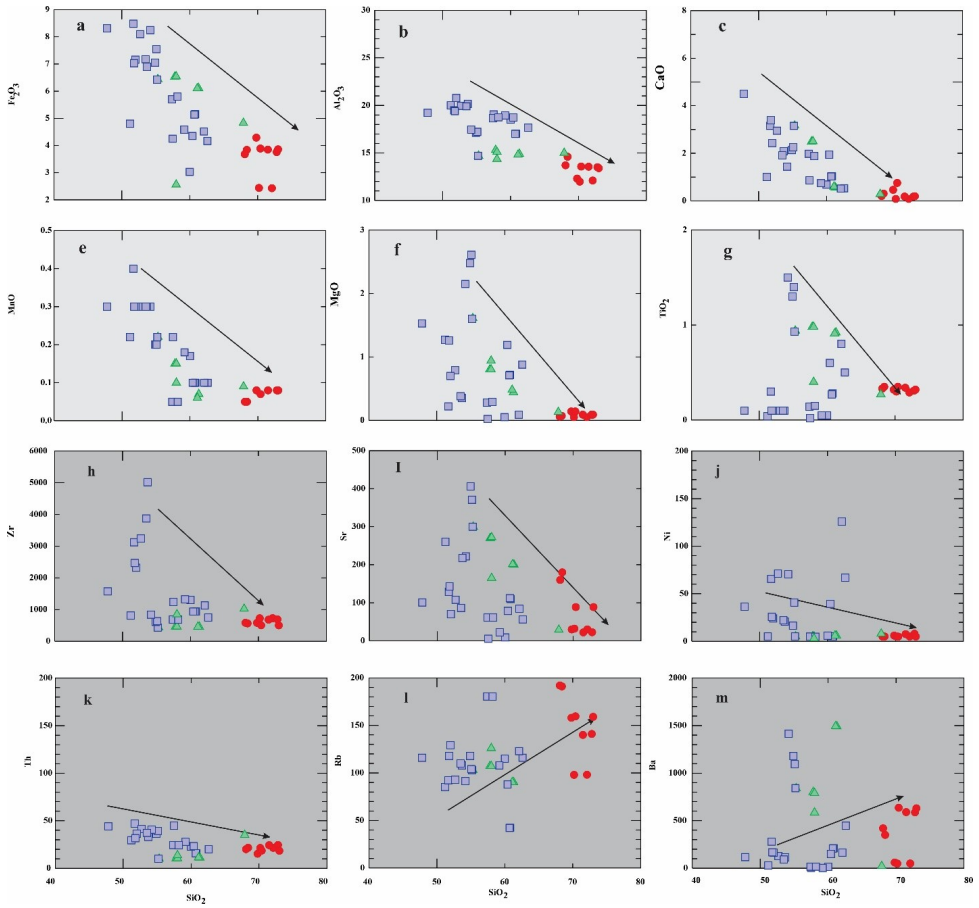

Figure 6. Harker diagrams variation of the major oxides and trace elements vs. SiO_2 of the studied samples. Symbols are the same as in Fig. 5.

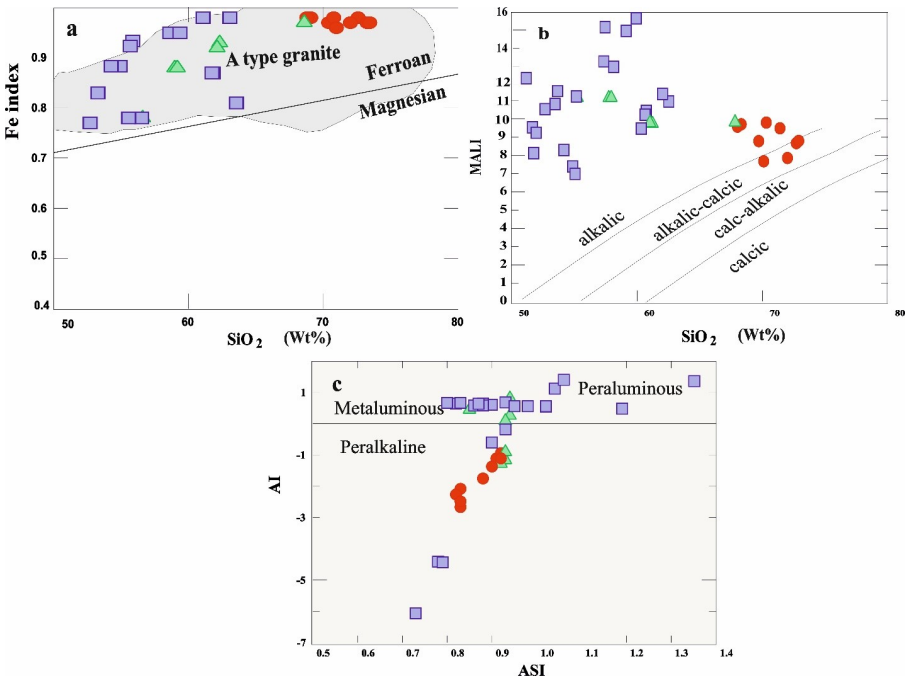

Figure 7. Eshkavarat granitoid samples on the diagram of (A): SiO_2 vs. Fe-Index boundary between Ferroan and magnesian rocks from Frost and Frost (2008); (B): MALI vs. SiO_2 boundary between alkali, alkali-calcic, calc-alkalic and calcic granitoids from Frost et al. (2001) and (C): AI vs ASI (comparing the differentiation trends of peralkaline granitoids with those of volcanic rocks at Boina (Barberi et al., 1975) and Nyambeni (Brotzu et al., 1983). Symbols are the same as in Fig. 5.

alkaline to relatively alkaline, anhydrous and non-orogenic (Wang et al., 2020). A-type granites, compared to other orogenic granites, have a high FeOt/MgO ratio (indicative of their origin) and a high Na_2O+K_2O content (high alkalinity), high (Na+K)/Al and K/Na ratios, high values of Nb, Y, Zn, F, Ga, Zr, REEs except (Eu), low ratio of LILE/HFSE, low values of MgO, CaO, Ni, Cr and Al_2O_3, and so they are different from I and S type granitoids (Martin, 2006; Bonin, 2007; Dargahi et al., 2010; Deng et al., 2016). A-type granitoids are small in volume and are found scattered throughout orogenic belts, sometimes in extensional tectonic regimes following major orogeny as a result of post-orogenic uplift and erosion. As a result, these granitoids are either non-orogenic or are replaced in non-compressive environments and at the end of the orogenic cycle as post-orogenic or post-collisional granitoids (Zhang et al., 2007; Xu et al., 2007; Dargahi et al., 2010).

Several petrogenetic models have been proposed for the

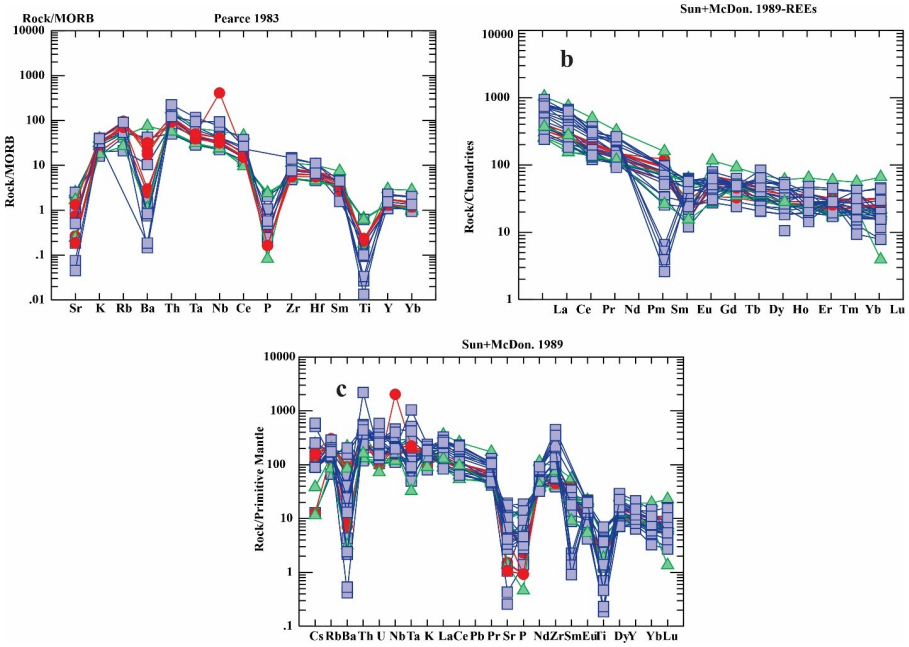

Figure 8. Abundances of REEs in Eshkavarat granitoid samples normalised to (a): MORB (Pearce, 1983); (b): Average chondrite (Sun and McDonough, 1989), (c): The primitive mantle (Sun and McDonough, 1989). Symbols are the same as in Fig. 5.

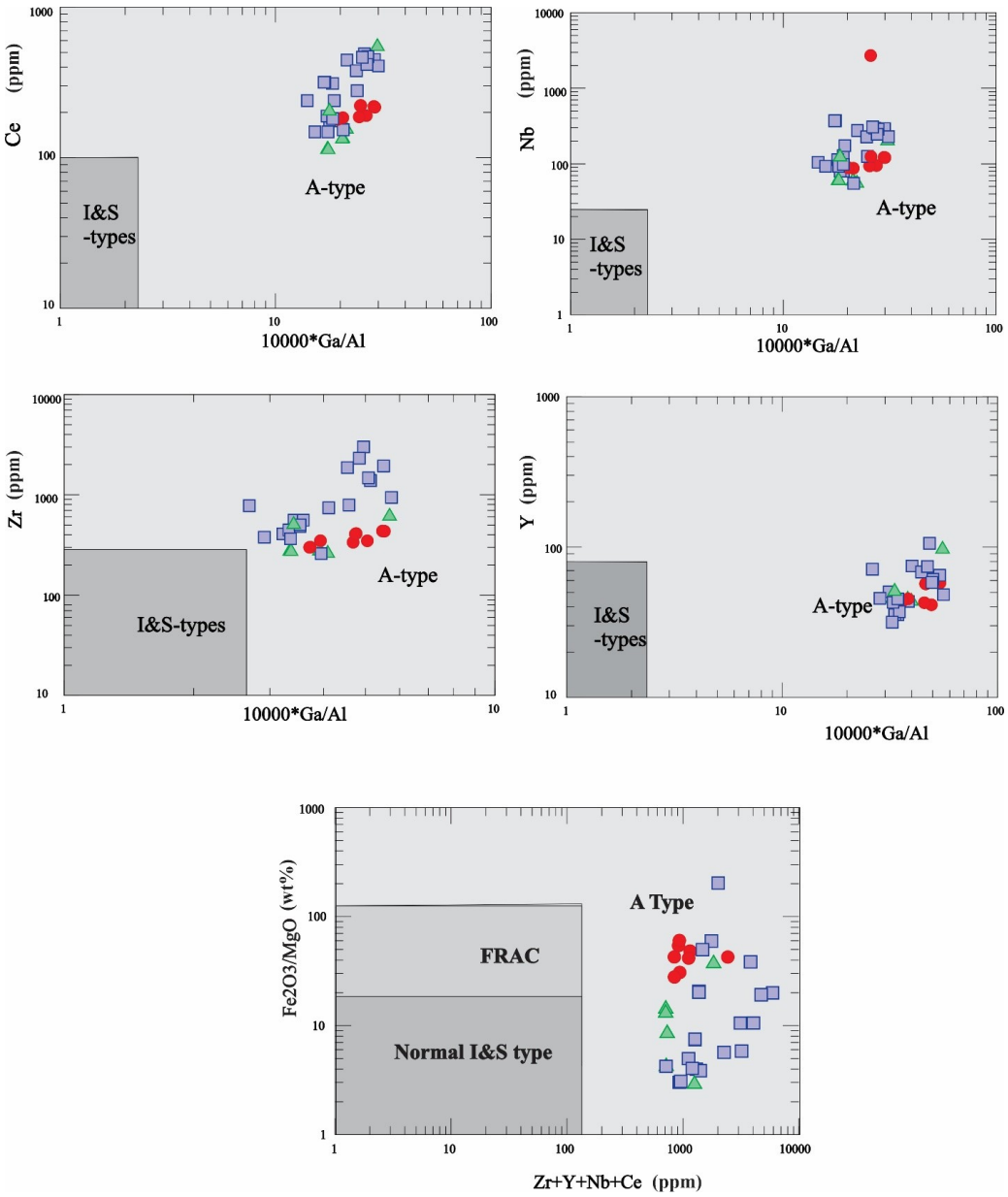

Figure 9. Eshkavarat granitoid samples on discrimination diagrams based on Ga/Al vs. (Y, Ce, Nb and Zr) and Zr+Nb+Ce+Y vs. $FeO_{(total)}$/MgO (Whalen et al., 1987). Symbols are the same as in Fig. 5.

A-type granites, mainly including:

(A) *Fractional crystallization from mantle-derived mafic magmas (Turner et al., 1992; Han et al., 1997; Chen and Arakawa, 2005).*

(B) *Partial melting of crustal rocks (Collins et al., 1982; Creaser et al., 1991; Huang et al., 2012).*

(C) *Interaction between mantle-derived magmas and overlying crustal rocks (magma mixing) (Kerr and Fryer, 1993; Griffin et al., 2002);*

Based on the available geological and geochemical results, the possibility of each model for the studied rocks is evaluated below.

5.1.1 Fractional crystallization from mantle-derived mafic magmas

The field relationships and relative ages between the alkaline OIB mafic rocks and the granitic rocks show that the A_1 granitoids were emplaced after the alkaline OIB mafic rocks. Therefore, it appears that the studied A_1-type granitoids are spatially and temporally related to the alkaline OIB mafic complex, but, in other words, it is possible that the studied granitoids are derived from intense fractionation of the alkaline OIB mafic magma. Meanwhile, the Harker diagrams (Figures 13 and 14) show a daly gap between the alkaline OIB mafic rocks and the Eshkavarat granitoids. On the other hand, considering that the ratios of rare earth elements (such as Nb/U, Rb/La, Zr/Hf) are different between the alkaline OIB mafic rocks and the studied granitoid rocks, and with the increase of SiO_2, the major and rare earth elements and the ratio They show different evolutionary trends

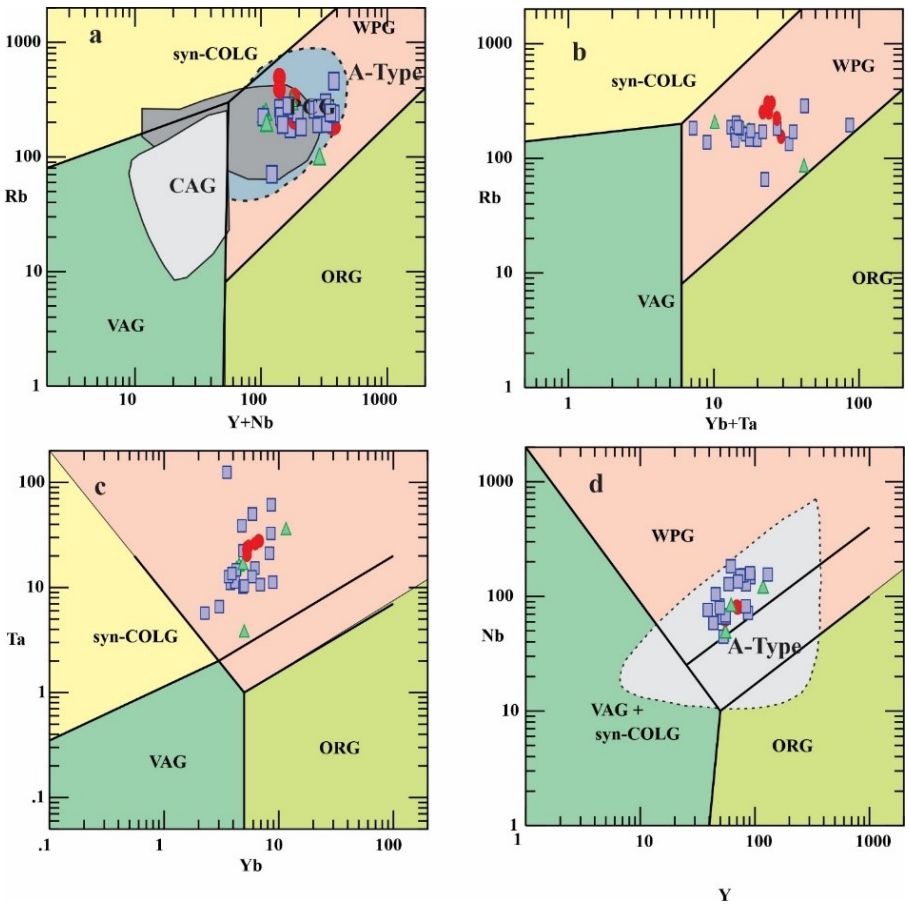

Figure 10. Discriminant diagrams of trace elements (Pearce et al., 1984): (A): Rb versus Y+Nb; (B): Rb versus (Yb + Ta); (C): Ta vs. Yb and D: Nb vs. Y. ORG = oceanic ridge granites, VAG = volcanic arc granites, WPG = within-plate granites, COLG = collisional granites. Symbols are the same as in Fig. 5.

for the studied granitoid mafic rocks and the alkaline OIB mafic, so the differentiation process of the alkaline OIB mafic rocks cannot explain the formation of the studied granitoids. Therefore, it appears that the mantle-derived mafic magma that formed the alkaline OIB mafic rocks in the region did not directly contribute to the formation of the Eshkorate granitoids.

5.1.2 Partial melting of crustal rocks

Partial melting of crustal rocks is one of the processes involved in the formation of granites, but in the case of the granitoids studied, partial melting of the young lithospheric mantle alone cannot explain the low Mg# content (< 0.4) and the relative enrichment of Hf and Zr elements, because the felsic rocks originating from the lithospheric mantle are depleted of HFSE and show high Mg# values (> 0.4) (Rapp

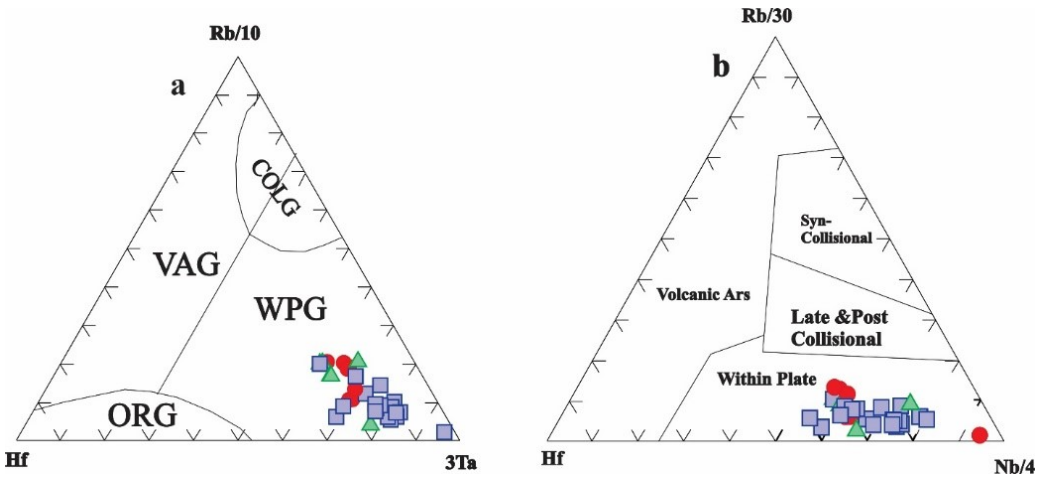

Figure 11. Eshkavarat granitoid samples on the tectonic separated diagram of granitoids (Harris et al., 1986). Symbols are the same as in Fig. 5.

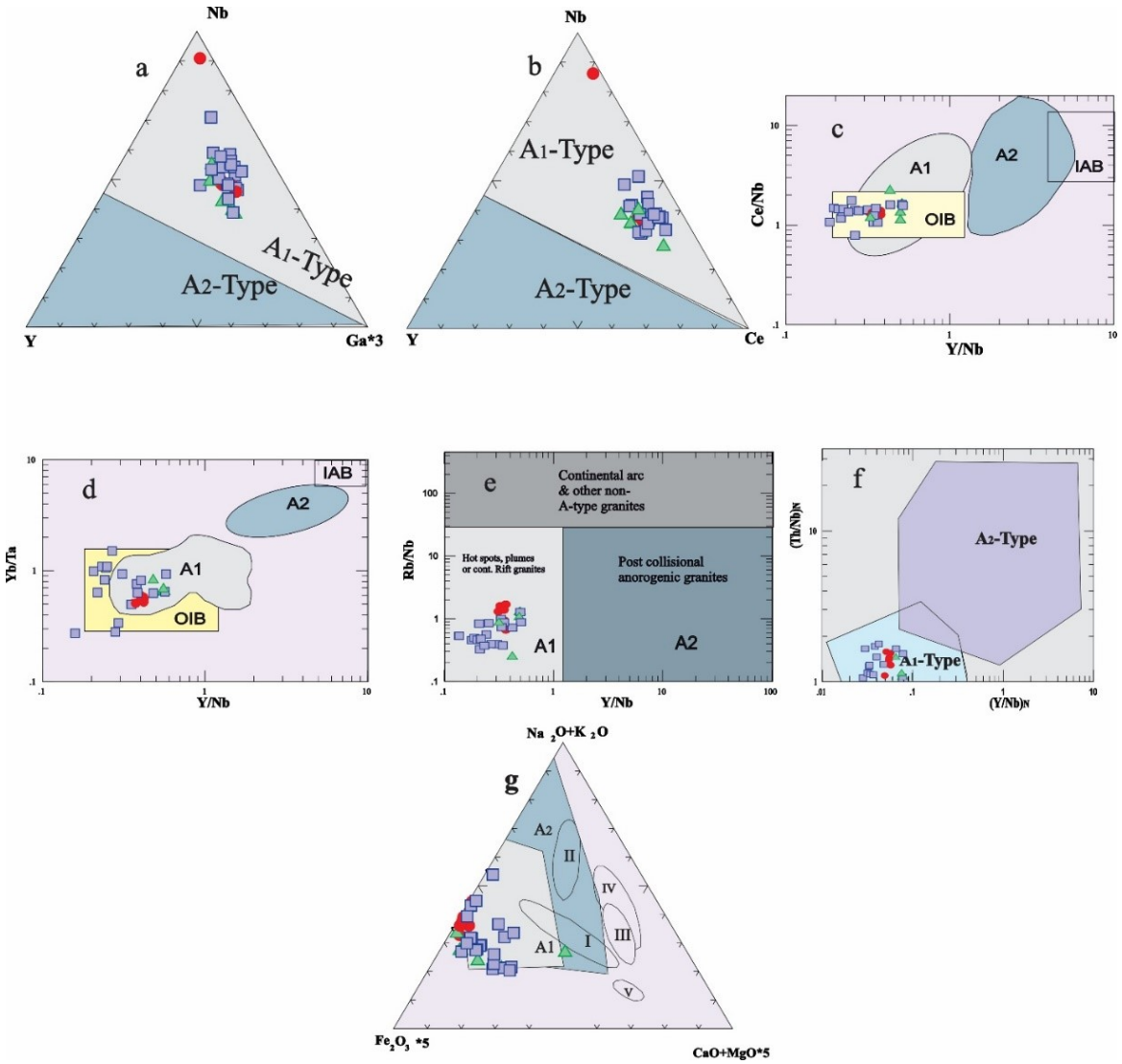

Figure 12. (A): Nb-Y-3*Ga and (B): Nb-Y-Ce discriminant diagrams of granitoids yielded from mantle sources (A_1) and crustal sources (A_2) (after Eby (1992)); (C), (D): Separation of OIB and IAB fields based on Ce/Nb and Yb/Ta vs. Y/Nb and Rb/Nb vs. Y/Nb; (E): (Eby, 1992); (F): Eshkavarat granitoid samples on the diagram of Y/Nb vs. Th/Nb (Moreno et al., 2014) normalized to Silicate Earth (McDonough and Sun, 1995); (G): On diagram (Na_2O+K_2O)–$Fe_2O_3\times5$–(CaO+MgO)×5 (mol. quant.). A_1 and A_2 Fields are from Grebennikov (2014), I, zones of mantle plumes in oceanic plates (oceanic islands and lava plateaus); II, intracontinental rifts and continental hot spots; III and IV, zones of subduction processes III, zones of island-arc magmatism in oceanic crust; IV, zones of magmatism of active continental margins, involving continental crust in magma formation; V, back-arc spreading. Symbols are the same as in Fig. 5.

and Watson, 1995; Chen and Arakawa, 2005).

Based on the field relationships, the partial melting of underplated rocks at the crust-mantle interface caused by the OIB plume is proposed as an acceptable source for the formation of the studied granitoids. As this source was derived from a relatively depleted mantle, just before partial melting, the magmas derived from it show the geochemical characteristics of depleted mantles.

Fractional crystallisation also played an important role in the generation of the Eshkavarat A_1 granitoids, in addition to the partial melting process. Cao, FeO*, MgO, Cr and Ni contents decrease with increasing SiO_2 contents from A_1-type syenitic rocks to A_1-type granitic rocks (Fig. 6). This reflects the fractionation of ferromagnesian minerals (such as pyroxene and biotite). Compatible (e.g. V, Ni) versus incompatible (e.g. Rb) element classification plots further support the fractionation crystallisation model (Li et al., 2022). These samples predominantly follow the decreasing trend of compatible versus incompatible elements (Fig. 15 a). The Rb and Rb/Sr ratio (Wu et al., 2021) is positively correlated with Sr (Fig. 15 b, c), suggesting that there is separation crystallisation of clinopyroxene and biotite in the magmatic evolution, also the samples of alkali granite show the fractional crystallization of plagioclase and K-feldspar.

The reduction of TiO_2 with SiO_2, the relatively high concentrations of Nb and Ta, and the negative anomalies of Ti are indicative of the crystallisation of ilmenite, with little influence from rutile or titanite (Xiong et al., 2005; Su et al., 2013). Rutile and titanite usually have higher partition coefficients for Nb and Ta than ilmenite (Xiong et al., 2005; Bédard, 2006). Also, In the $(La/Yb)_N$ versus La diagram (Fig. 15 d), clearly shows the separation crystallisation of apatite and titanite. The A_1 granites show Eu, Sr, Ba and

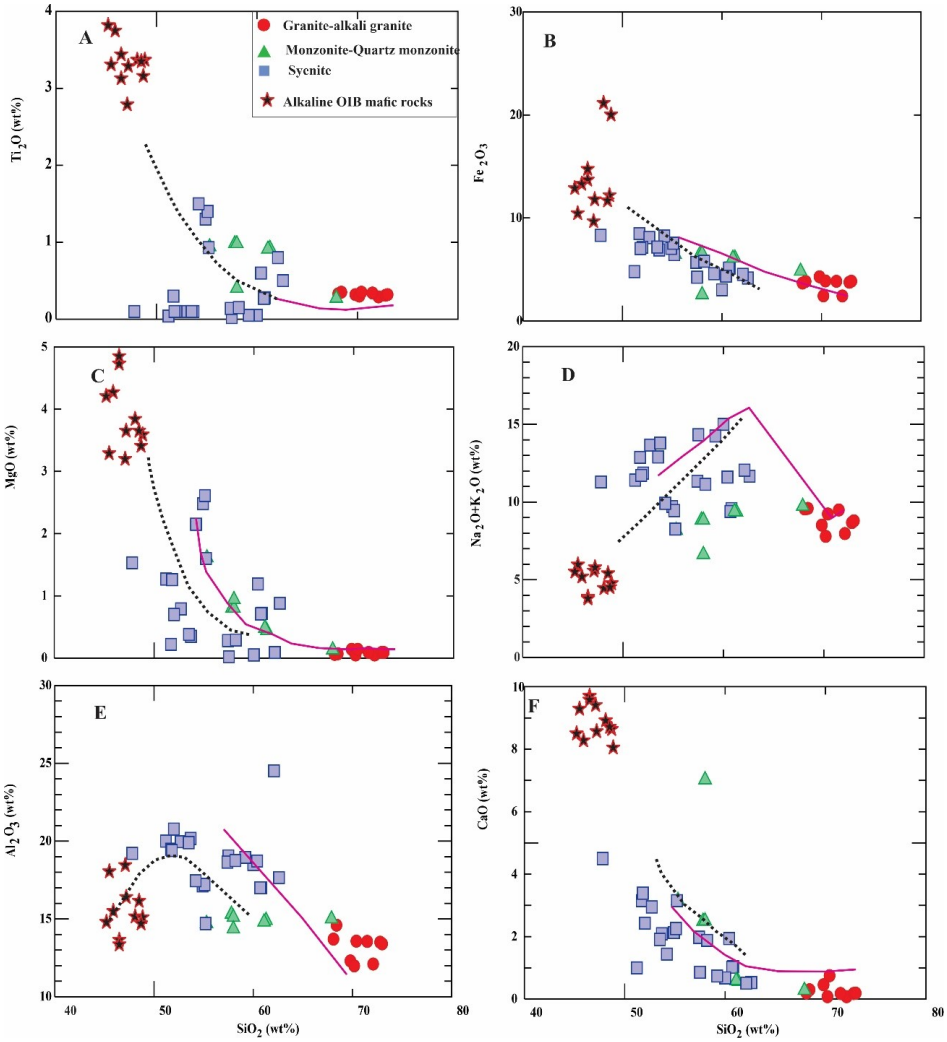

Figure 13. Harker diagrams for the investigated granitoids and alkaline OIB mafic rocks and comparison of the magma evolution process of the investigated granitoids. Each of them show different evalution trend. The dark dotted lines show the melt evolution trend for the partial melting modelling and the pink lines for the fractional crystallization modelling. OIB mafic data from Salavati et al. (2013).

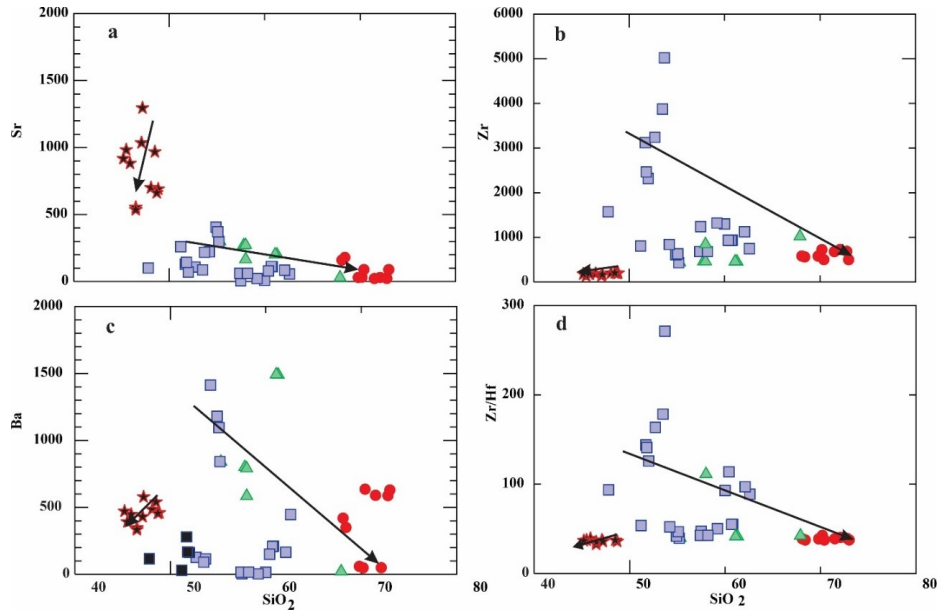

Figure 14. Harker diagrams of the Eshkavarat granitoids and OIB-mafic rocks, Each rock group shows a separate evolution trend. Symbols are the same as Fig. 13. OIB mafic data from Salavati et al. (2013).

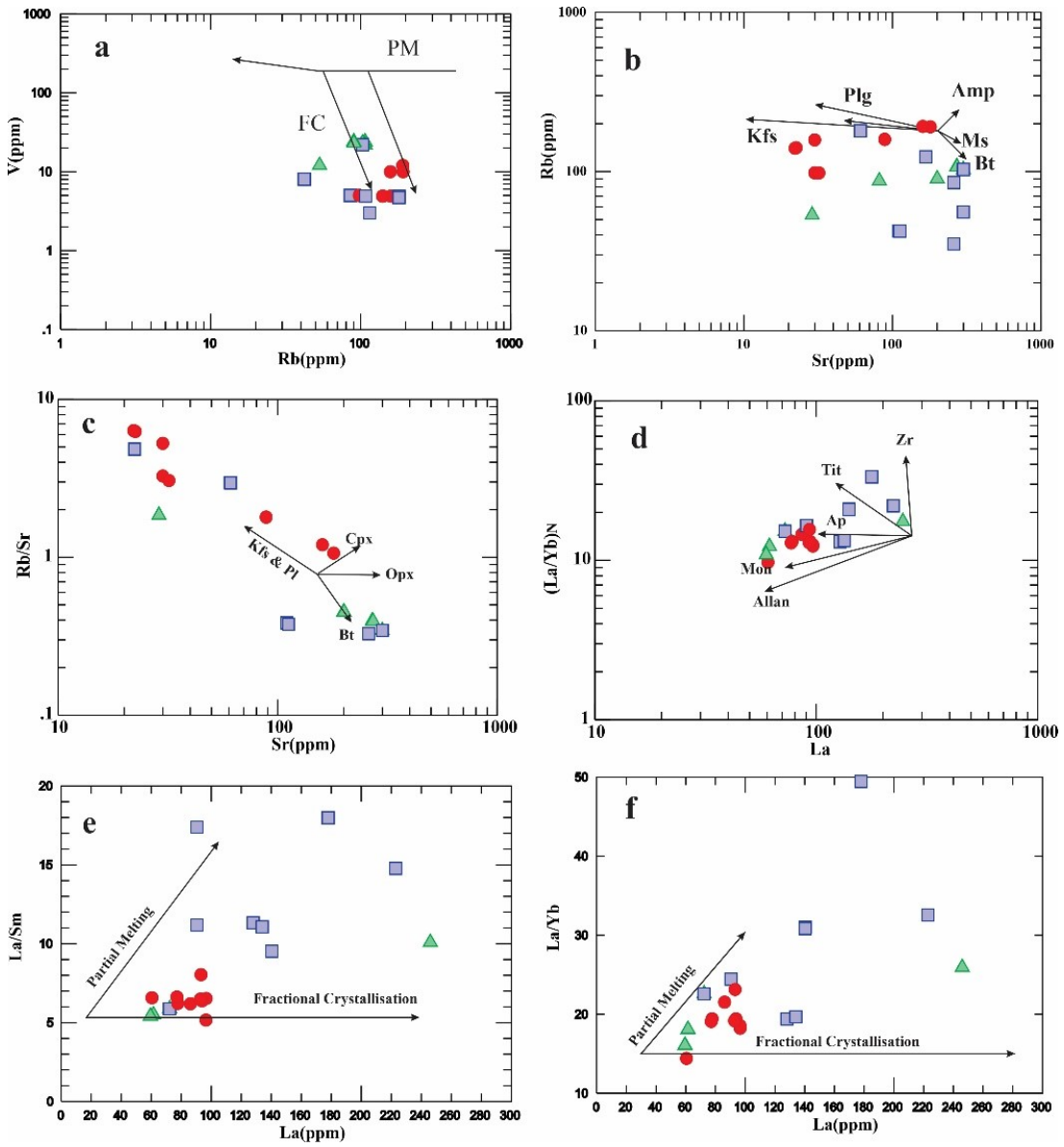

Figure 15. Chemical discrimination diagrams illustrating the mineral fractionation crystallization and partial melting trend for Eshkavarat granitoid samples; (a): V vs. Rb showing fractional crystallization (after Schiano et al. (2010)); (b): Rb vs. Sr (Wang et al., 2020); (c), (d): Rb vs. Rb/Sr and La vs. $(La/Yb)_N$ (Wu et al., 2021); (c), (d): La vs. La/Sm and La vs. La/Yb for studied granitoids showing partial melting and fractional crystallization (Fan et al., 2021). Symbols are the same as in Fig. 5. Pl = plagioclase; Kfs = K-feldspar; Amp = amphibole; Ms = muscovite; Bt = biotite; Cpx = clinopyroxene; Opx = orthopyroxene; Zr = zircon; Tit = titanite; Ap = apatite; Mon = monazite; and Allan = allanite.

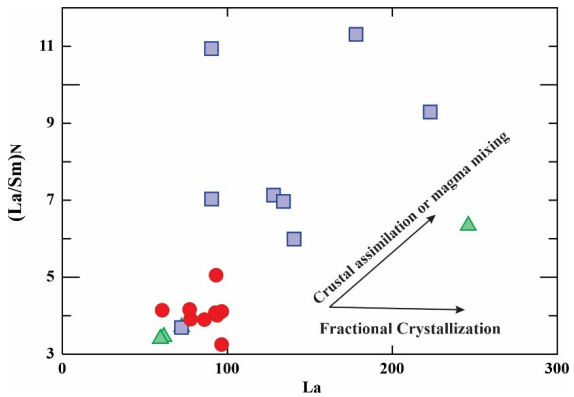

Figure 16. La contents versus $(La/Sm)_N$ ratios (Wang et al., 2020) for the Eshkavarat granitoids. Symbols are the same as in Fig. 5.

P negative anomalies in the spider patterns (Fig. 6), suggesting that plagioclase, K-feldspar and apatite minerals were also separated during magmatic evolution. Although the crystallisation and segregation of the above minerals occurred during the magmatic evolution process, the evolutionary process, La versus La/Sm and La versus La/Yb diagrams (Fig. 15 e, f) show that the formation of syenite is mainly controlled by partial melting, so that the nature of the has a more important influence on the composition of the magma.

5.1.3 Interaction between mantle-derived magmas and overlying crustal rocks (magma mixing)

Magma mixing between mafic mantle-derived magmas and more felsic crustal melts has been proposed as an effective way to generation of granitoids (Griffin et al., 2002; Yang

et al., 2006). The interaction between mantle-derived magmas and crustal felsic melts causes a decrease in the SiO_2 content of the original felsic melts, and this may explain the low silica nature of the granitoids studied. Thus, magma mixing is observed in the studied granitoid rocks, as indicated by field and lithological evidence such as mafic (basaltic) micro granular enclaves (Fig. 2 b). Therefore, magma mixing may be one of the effective processes used to form the Eshkavarat A_1 granitoids. Also, the slight increase between the $(La/Sm)_N$ and La content ratios (Wang et al., 2020) (Fig. 16) suggests that the Eshkavarat granitoids experienced some contamination or magma mixing during their formation.

A specific classification of felsic igneous rocks according to their petrochemical composition has been proposed by Frost et al. (2001). They used three chemical parameters as a basis for this:

(1) The Fe index $FeO^*/(FeO^*+MgO)>0.486+0.0046\times SiO_2$ (wt.%), which allows the separation of magnesian and ferroan (A-type) granitoids,

(2) the Peacock modified alkali-lime index (Na_2O+K_2O-CaO) (MALI),

and (3) the alumina saturation index (ASI) Al/(Ca-1.67-P+Na+K), which allows felsic igneous rocks to be classified as peraluminous (ASI > 1.0), meta-aluminous (ASI < 1.0, (Na+K) < Al) and peralkaline (ASI < 1.0, (Na+K) > Al). The formation of ferro-aluminous granitoids by partial crustal melting at low pressure was suggested by Frost and Frost (2008). Also, Peralkaline ferroan granitoids can be generated as a result of the subduction of alkaline basalts or transition basalts that may have been affected by crustal assimilation (Frost and Frost, 2008).

Thus, in the study area, we suggest that primitive granitoid parent magmas were generated by the first partial melting of underplated rocks (by magmas derived from the asthenospheric mantle, which is the source of the alkaline OIB mafic rocks). This was followed by the fractionation of mafic minerals to form syenitic magmas and then the fractionation of felsic minerals to form A_1-type granite and alkali granite that have been affected by crustal assimilation. A comparison of the studied granitoid and mafic rocks on the major element diagrams shows that the studied samples follow the modeled trends (Fig. 17).

6. Geodynamic implications

A-Type granitoids are found in a wide range of tectonic settings, including oceanic islands, continental rifts, extended crust, stable continental crust and post-orogeny (Whalen et al., 1987; Zhang et al., 2007; Xu et al., 2007). These granitoids are a special group of felsic intrusive rocks that are controversial due to their specific geochemistry, tectonic setting, and petrogenesis (Frost et al., 2001; Bonin, 2007; Forest and Forest, 2011; Yajam and Ghalamghash, 2019). Multiple processes and different crust/mantle ratios are responsible for the formation of A-type granitoids in different tectonic settings. This indicates the diversity and complexity of the processes and the models by which they are formed. These granitoids are indicators of rifting zones and the inner parts of continental plates (Blatt et al., 2006). They are often formed at the end of the magmatic or orogenic cycle in each state, after the formation of other granitoids. These types of granitoids can result from differential crystallisation of mafic mantle-derived magmas (Eby, 1992; Turner et al., 1992; Shellnutt et al., 2011); partial melting of the mantle source (Wu et al., 2002; Shellnutt and Zhou, 2007; Shellnutt et al., 2011); or a mixture of two end members (Yang et al., 2006; Pankhurst et al., 2013). Particularly where structural evidence and geochemical relationships have been lost or weakened by multiple deformation events, it is difficult to distinguish between non-orogenic and post-collisional granitoids.

As mentioned above, fractional crystallisation of mantle-derived melt could be involved in the genesis of the A_1-type granitoid. In this case, these granites are associated with large assemblages of mafic rocks (Forest and Forest, 2011). According to Eby (1992), A-type granitoids are divided

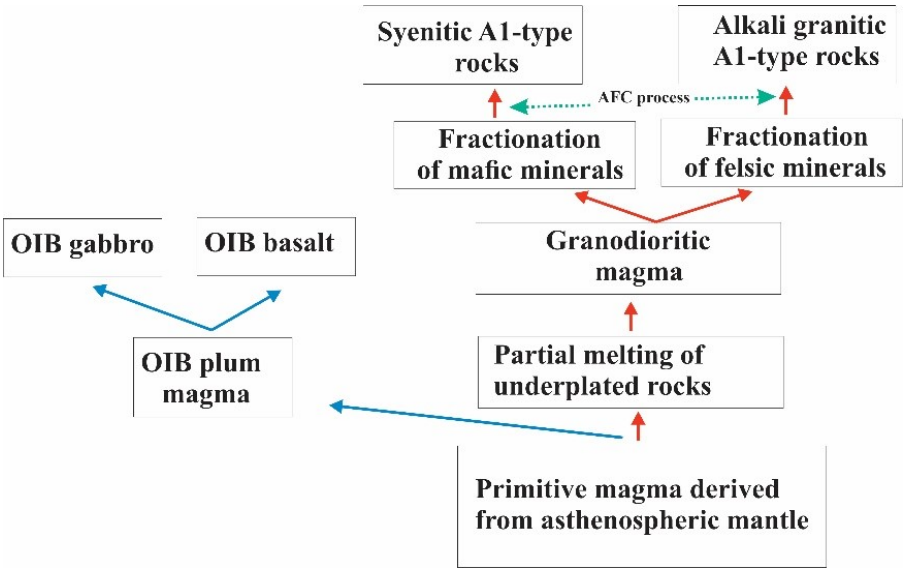

Figure 17. Proposed petrogenetic model for the generation of Eshkavarat A_1-type granitoids in the eastern Gilan.

into A_1 groups (similar to oceanic island basalts (OIBs) and mantle-origin rocks) and A_2 groups (formed from continental crusts or subducted crusts displaced by a cycle of continental-continental collision or island arc magmatism). A_1 types are positioned during rifting and are the result of plum or hot spot activity. A_2 types occur in a wide range of tectonic settings and include post-collisional granitoids and post-orogenic granitoids (granitoids that are at the end of a long period of heat flow and granitic magmatism) (Whalen et al., 1987; Eby, 1992). Based on all the geochemical evidence presented and other geological and tectonic evidence for the region, it appears that the granitoid bodies studied belong to the group of non-orogenic granitoids (A_1 -type).

Recent studies have shown that A-type granites can be generated in lithospheric window tectonic environments (slab window setting) (Eyuboglu et al., 2013; Zhang, 2014; Windley and Xiao, 2018; Wang et al., 2020). In these environments, subduction of an active and young mid-ocean ridge has been generated under the continental crust and as a lithospheric window environment (slab window setting) (Zhang, 2014; Windley and Xiao, 2018; Wang et al., 2020).

Plume-like rocks (OIB) are formed by upwelling of the asthenospheric magmas. The arrest of these asthenospheric magmas beneath the crustal plate can cause partial melting of the underplate and the formation of underplate magmas (probably of diorite composition). Fractional crystallisation of these resulting underplate magmas produces a non-orogenic A-type granitic tectonic setting, due to the upwelling of the asthenospheric mantle. Subduction rocks are similar to normal arc rocks and generally related adakitic rocks are also observed in such a tectonic setting, in addition to mantle rocks and their fractional products. Based on all the petrogenetic and tectonic data, a schematic petrogenetic and tectono-magmatism model is proposed for the formation of the A_1-type Eshkavrat granitoids (Fig. 18).

Cenozoic geodynamic setting in eastern Gilan, northern Iran, considering a post-collisional extension, intraplate setting and arc setting associated with Neo-Tethyan subduction.

Based on this model, we propose that the major Cenozoic magmatism in the northern Alborz in the southern Caspian Sea occurred by creating a slab window (at the same time of subduction). According to previous studies, the oceanic crust of the southern Caspian Sea, as part of the Tethyan oceanic crust, was subducted southwards beneath the North Alborz orogen (as part of the Pontid-Little Caucasus-Alborz magmatic arc in an active continental margin during the Cenozoic) (Eyuboglu et al., 2013).

This hot and young subducted oceanic plate, separated by transform faults and thus a small slab window, was created beneath the northern Alborz. Subsequently, the hot asthenospheric mantle ascended through the slab window beneath the subducted plate, creating an asthenospheric magma-filled gap between the divergent and subducted oceanic plates. Alkaline OIB mafic rocks were formed by fractionation and accumulation of magma from the plume (Zaeimnia et al., 2010; Salavati et al., 2013). At the same time, the arrest of this hot asthenospheric magma as a plume below the crust has caused the melting of part of the crust (SCLM: Sub-Continental Lithosphere Mantle). Partial melting of underplated rocks by upwelling asthenosphere, followed by fractionational crystalisation of mafic minerals and minor crustal assimilation, primarily generated parent magma of A_1 granitoids and syenitic A_1 rocks, and then the fractionation of felsic minerals with the effect of AFC processes causes the formation of A_1-type (alkaline) granites, and

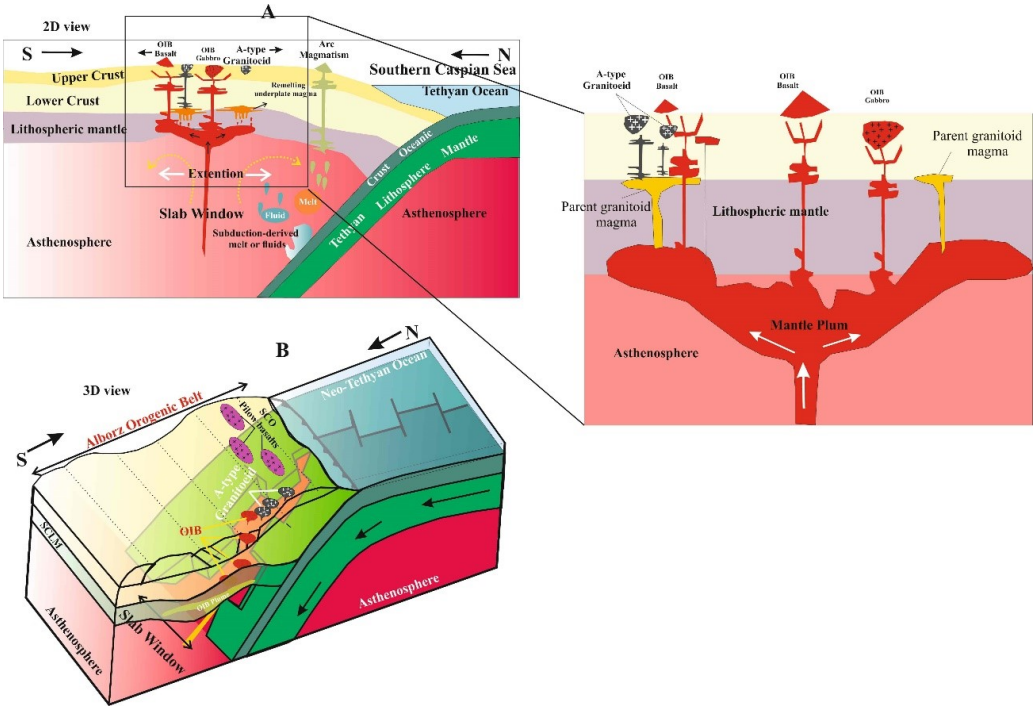

Figure 18. Proposed schematic diagram showing the tectonic setting and oceanic crustal conditions of the southern Caspian Sea during the Late Cretaceous and Early Palaeogene, and the proposed tectono-magmatism scenario for the formation of A-type granitoids in the eastern region of Gilan Province.

finally, the ascent and injection of this magma have formed studied A_1-type granitoid into the older rocks (alkaline OIB rocks of the region and rocks of the ophiolitic complex of the southern Caspian Sea).

7. Conclusion

- The main conclusions of this study, based on the geological and geochemical data as well as on the geodynamic setting of the granitoid rocks exposed in the Northern Zone of the Alborz Orogenic Belt, are presented below:

- The Eshkavarat granitoid rocks have a post-Eocene relative age based on the field relationship.

- Petrographic studies represent various monzonite, quartz monzonite to granite in these rocks. The dominant texture of these rocks is granular to porphyry-granular. Perthitic, graphic and poikilitic textures are less common.

- The Eshkavarat granitoid rocks in the chondrite-normalised spider diagram show subparallel, linear and homogeneous REE profiles. They also have high enrichments of LILE elements such as K, Rb and Th, indicating the existence of an enriched mantle source beneath the continental lithosphere (metasomatised mantle).

- Based on major and REE geochemical data, the Eshkavarat granitoid rocks have the characteristics of WPG A-type granitoids formed in a post-collisional setting.

- The samples are more peralkaline and less peraluminous and based on the geochemical data, the Eshkavarat granitoid rocks are A_1-type.

- The process of partial melting and crystal fractionation has played an important role in the generation of Eshkavarat A_1-type granitoids.

- All the evidence suggests that the studied granitoids were formed as a result of slab-window activation above the supra-subduction zone at the same time as the ophiolitic complex was formed in the southern Caspian Sea area.

- Upwelling of mantle magma from the slab window and an oceanic plume, alkaline OIB magmatism was activated during the subduction of the Neo-Tethyan oceanic crust. Then, partial melting of part of the underplated rocks generated parental magma. Fractional crystalisation of mafic minerals of this magma and minor crustal assimilation of the parent magma generated A_1-type granitic and syenitic and then, the fractionation of felsic minerals with the effect of AFC processes generated the A_1-type alkaline granites.

Acknowledgments

The present study is the result of a study entitled "Petrology and Geochemistry of Eshkavarat Dome in East Gilan, North Iran" and the authors would like to thank the Office of Graduate Studies of Islamic Azad University, Lahijan Branch.

Authors contributions
All the authors have participated sufficiently in the intellectual content, conception and design of this work or the analysis and interpretation of the data (when applicable), as well as the writing of the manuscript.

Availability of data and materials
The data that support the findings of this study are available from the corresponding author, upon reasonable request.

Conflict of interests
The authors declare that they have no known competing financial interests or personal relationships that could have appeared to influence the work reported in this paper.

References

Aghanabati A. (2006) Geology of Iran. *Geological Survey of Iran*

Alirezaei S., Hassanzadeh J. (2012) Geochemistry and zircon geochronology of the Permian A-type Hasanrobat granite, Sanandaj-Sirjan belt: A new record of the Gondwana break-up in Iran. *Lithos* 151:122–134. DOI: https://doi.org/10.1016/j.lithos.2011.11.015.

Arslan M., Aslan Z. (2006) Mineralogy, petrology, and whole-rock geochemistry of the Tertiary granitic intrusions in the Eastern Pontides. *Turkey Journal of Asian Earth Sciences* 27 (2): 177–193. DOI: https://doi.org/10.1016/j.jseaes.2005.03.002.

Asiabanha A., Foden J. (2012) Post-collisional transition from an extensional volcano-sedimentary basin to a continental area in the Alborz Ranges, N-Iran. *Lithos* 148 (1): 98–111. DOI: https://doi.org/10.1016/j.lithos.2012.05.014.

Azizi H., Kazemi T., Asahara Y. (2017) A-type granitoid in Hasansalaran complex, northwestern Iran: Evidence for extensional tectonic regime in northern Gondwana in the Late Paleozoic. *Journal of Geodynamics* 108:56–72. DOI: https://doi.org/10.1016/j.jog.2017.05.003.

Baharfiruzi Kh., Shafeii A. R. (2003) Geological map of Javaherdeh. *Geological Survey of Iran, Tehran* 1:100000.

Barberi F., Ferrara G., Santacroce R., Treuil M., Varet J. (1975) A transitional basalt-pantellerite sequence of fractional crystallization, the Boina center (Afar Rift, Ethiopia). *Journal of Petrology* 16:22–56. DOI: https://doi.org/10.1093/petrology/16.1.22.

Berberian M., King G. C. P. (1981) Towards a paleogeography and tectonic evolution of Iran. *Canadian Journal of Earth sciences* 2:210–265. DOI: https://doi.org/10.1139/e81-019.

Blatt H., Tracy R. J., Owens B. E. (2006) Petrology: Igneous, Sedimentary, and Metamorphic. *United States: Freeman and Company*

Bonin B. (2007) A-type granites and related rocks: Evolution of a concept, problems, and prospects. *Lithos* 97:1–29. DOI: https://doi.org/10.1016/j.lithos.2006.12.007.

Brotzu P., Morbidelli L., Piccirillo E. M. (1983) The basanite to peralkaline phonolite suite of the Plio-Quaternary Nyambeni multicenter volcanic range (East Kenya Plateau). *Neues Jahrbuch fur Mineralogy, Abhandlungen* 147:253–280.

Bédard J. H. (2006) A catalytic delamination-driven model for coupled genesis of Archean crust and sub-continental lithospheric mantle. *Geochimica et Cosmochimica Acta* 70:1188–214.

Chen B., Arakawa Y. (2005) Elemental and Nd-Sr isotopic geochemistry of granitoids from the West Junggar foldbelt (NW China), with implications for Phanerozoic cintinental growth. *Geochimica et Cosmochimica Acta* 69 (5): 1307–20.

Collins W. J., Beams S. D., White A. J. R., Chappell B. W. (1982) Nature and origin of A-type granites with particular reference to southeastern Australia. *Contributions to Mineralogy and Petrology* 80:189–200.

Cox K. G., Bell J. D., Pankhurts R. J. (1979) The interpretation of igneous rocks. *London, United Kingdom: Chapman & Hal*

Creaser R. A., Price R., Wormald R. J. (1991) A-type granites revisited: assessment of a residual- source modal. *Geology* 19:163–6.

Dabiri R., Akbari-Mogaddam M., Ghaffari M. (2018) Geochemical evolution and petrogenesis of the eocene Kashmar granitoid rocks, NE Iran: Implications for fractional crystallization and crustal contamination processes. *Iranian Journal of Earth Sciences* 10 (1): 68–77.

Dargahi S., Arvin M., Pan Y., Babaei A. (2010) Petrogenesis of post-collisional A-type granitoids from the Urumieh-Dokhtarmagmatic assemblage, SouthwesternKerman, Iran: Constraints on the Arabian-Eurasian continental collision. *Lithos* 115:190–204. DOI: https://doi.org/10.1016/j.lithos.2009.12.002.

De La Roche H., Leterrier J., Grandclaude P., Marchal M. (1980) A classification of volcanic and plutonic rocks using R1R2-diagram and major element analyses its relationships with current nomenclature. *Chemical Geology* 29:183–210. DOI: https://doi.org/10.1016/0009-2541(80)90020-0.

Deng X., Peng T., Zhao T. (2016) Geochronology and geochemistry of the late Paleoproterozoic aluminous A-type granite in the Xiaoqinling area along the southern margin of the North China Craton: Petrogenesis and tectonic implications. *Precambrian Research* 285:127–146. DOI: https://doi.org/10.1016/j.precamres.2016.09.013.

Eby G. N. (2011) A-type granites: magma sources and their contribution to the growth of the continental crust. *Seventh Hutton symposium on granites and related rocks, Avila, Spain*

——— (1992) Chemical subdivision of the A-type granitoids, petrogenetic and tectonic implications. *Geology* 20:641–644. DOI: https://doi.org/10.1130/0091-7613(1992)020$¡$0641:CSOTAT$¿$2.3.CO;2.

Ernst R. E. (2014) Large igneous provinces. *Cambridge, United Kingdom: Cambridge University Press,* DOI: https://doi.org/10.1017/CBO9781139025300.

Eyuboglu Y., Santosh M., Dudas F. O., Akaryal E., Chung S. L., Akdag K., Bektas O. (2013) The nature of transition from adakitic to non-adakitic magmatism in a slab window setting: A synthesis from the eastern Pontides, NE Turkey. *Geoscience Frontiers* 4:353–375.

Fan X. Z., Sun F. Y., Xu C. H., Wu D. Q., Yu L., Wang L., Yan C., Bakht S. (2021) Volcanic rocks of the Elashan Formation in the Dulan-Xiangride Basin, East Kunlun Orogenic Belt, NW China: Petrogenesis and implications for Late Triassic geodynamic evolution. *International Geology Review* 64:1270–1293.

Foley S. F., Wheller G. E. (1990) Parallels in the origin of the geochemical signatures of island arc volcanics and continental potassic igneous rocks: the role of residual titanates. *Chemical Geology* 85:1–18. DOI: https://doi.org/10.1016/0009-2541(90)90120-V.

Forest C. D., Forest B. R. (2011) On Ferroan (A-type) granitoids: their compositional variability and modes of origin. *Journal of Petrology* 52:39–53. DOI: https://doi.org/10.1093/petrology/egq070.

Frost B. R., Arculus R. J., Barnes C. G., Collins W. J., Ellis D. J., Frost C. D. (2001) A geochemical classification of granitic rocks. *Journal of Petrology* 42:2033–2048. DOI: https://doi.org/10.1093/petrology/42.11.2033.

Frost B. R., Frost C. D. (2008) A geochemical classification for feldspathic igneous rocks. *Journal of Petrology* 49:1955–1969. DOI: https://doi.org/10.1093/petrology/egn054.

Ghaffari M., Rashidnejad-Omran N., Dabiri R., Santos J. F., Mata J., Buchs D., McDonald L., Appel P., Garbe-Schonberg D. (2015) Interaction between felsic and mafic magmas in the Salmas intrusive complex, Northwestern Iran: Constraints from petrography and geochemistry. *Journal of Asian Earth Sciences* 111:440–458. DOI: https://doi.org/10.1016/j.jseaes.2015.06.019.

Grebennikov A. V. (2014) A-type granites and related rocks: petrogenesis and classification. *Journal of Geodynamic* 55:1074–1086. DOI: https://doi.org/10.1016/j.rgg.2014.08.003.

Griffin W. L., Wang X., Jackson S. E., Pearson N. J., O'Reilly S. Y., Xu S., Zhou X. M. (2002) Zircon chemistry and magma mixing, SE China: in-situ analysis of HF isotopes, Tonglu and Pingtan igneous complexes. *Lithos* 61:237–69.

Han B. F., Wang S. G., Jahn B. M., Hng D. W., Kagami H., Sun Y. L. (1997) Depleted-mantle source for the Ulungur River A-type granites from North Xinjiang, China: geochemistry and Nd-Sr isotopic evidence, and implications for Phanerozoic crustal growth. *Chemical Geology* 138:135–59.

Hari K. R., Manu Prasanth M. P., Swarnkar V., Vijaya Kumar J., Randive K. R. (2018) Evidence for the Contrasting Magmatic Conditions in the Petrogenesis of A-type Granites of Phenai Mata Igneous Complex: Implications for Felsic Magmatism in the Deccan Large Igneous Province. *Journal of the Indian Institute of Science* 98:379–399. DOI: https://doi.org/10.1007/s41745-018-0079-z.

Harris N. B. W., Pearce J. A., Tindle A. G. (1986) Geochemical characteristics of collision-zone magmatism. *Geological Society, London, Special Publications* 19:67–81. DOI: https://doi.org/10.1144/GSL.SP.1986.019.01.04.

Honarmand M., Li X. H., Nabatian G., Neubauer F. (2017) In-situ zircon U-Pb age and Hf-O isotopic constraints on the origin of the Hasan-Robat A-type granite from Sanandaj-Sirjan zone, Iran: Implications for reworking of Cadomian arc igneous rocks. *Mineralogy and Petrology* 111:659–675. DOI: https://doi.org/10.1007/s00710-016-0490-y.

Huang H., Zhang Z., Kusky T., Santosh M., Zhang S., Zhang D., Liu J., Zhao Z. (2012) Continental vertical growth in the transitional zone between South Tianshan and Tarim, western Xinjiang, NW China: insight from the Permian Halajun A1-type granitic magmatism. *Lithos* 155L:49–66.

Ilbeyli N., Pearce J. A., Thirlwall M. F., Mitchell J. G. (2004) Petrogenesis of collision-related plutonics in Central Anatolia, Turkey. *Lithos* 72:163–182. DOI: https://doi.org/10.1016/j.lithos.2003.10.001.

Jiang X. Y., Wu K., Luo J. P., Zhang L. P., Sun W. D., Xia X. P. (2020) An A1-type granite that borders A2-type: insights from the geochemical characteristics of the Zongyang A-type granite in the Lower Yangtze River Belt, China. *International Geology Review Volume* 62:2203–2220. DOI: https://doi.org/10.1080/00206814.2019.1689534.

Kalantari K., Kananian A., Asiabanha A., Eliassi M. (2008) Source and tectonic setting of zarjebostan (NE OF Qazvin) Paleogene volcanic rocks using REE and HFSE elements. *Geosciences Scientific Quarterly Journal* 17:140–149. DOI: https://doi.org/10.22071/GSJ.2009.57853.

Kerr A., Fryer B. J. (1993) Nd isotope evidence for crust-mantle interaction in the generation of A-type granitoid suites in Labrador, Canada. *Chemical Geology* 104

Li S. S., Zeng W., Zhang H. F., Wang L., Shivute E. T., Qiu K. F. (2022) Fractional crystallization and partial melting of the Paleoproterozoic gneisses and pegmatite in the Giant Husab uranium deposite, Namibia. *Minerals* 12:379. DOI: https://doi.org/10.3390/min1203037939-60.

Martin R. F. (2006) A-type granites of crustal origin ultimately result from open-system fenitization-type reactions in an extensional environment. *Lithos* 91:125–136.
DOI: https://doi.org/10.1016/j.lithos.2006.03.012.

McDonough W. F., Sun S. S. (1995) The composition of the Earth. *Chemical Geology* 120:223– 253.
DOI: https://doi.org/10.1016/0009-2541(94)00140-4.

Middlemost E. A. K. (1985) Magmas and magmatic rocks. An introduction to igneous petrology. *London, United Kingdom: Longman*

Moine-Vaziri H. (1985) Volcanisme tertiaire et quaternaire en Iran. *PhD, University of Paris, France*

Mollai H., Dabiri R., Torshizian H. A., Pe-Piper G., Wang W. (2021) Upper Neoproterozoic garnet-bearing granites in the Zeber-Kuh region from east central Iran micro plate: Implications for the magmatic evolution in the northern margin of Gondwanaland. *Geologica Carpathica* 72 (6): 461–481.
DOI: https://doi.org/10.31577/GeolCarp.72.6.2.

Moreno J. A., Molina J. F., Montero P., Anbar M., Scarrow J. H., Cambeses A., Bea F. (2014) Unraveling sources of A-type magmas in junvenile continental crust: Constraints from compositionally diverse Ediacaran post-collisional granitoids in the Katerina Ring Complex, Southern Sinai, Egypte. *Lithos* 192-195:56–85.
DOI: https://doi.org/10.1016/j.lithos.2014.01.010.

Nazari M., Arian M. A., Solgi A., Zareisahamieh R., Yazdi A. (2023) Geochemistry and tectonomagmatic environment of Eocene volcanic rocks in the Southeastern region of Abhar, NW Iran. *Iranian Journal of Earth Sciences* 15 (4): 228–247.
DOI: https://doi.org/10.30495/ijes.2023.1956689.1746.

Ousta S. H., Ashja-Ardalan A., Yazdi A., Dabiri R., Arian M. A. (2024) Petrogenesis and tectonic implications of Miocene dikes in the southeast of Bam (SE Iran): Constraints on the development of active continental margin. *Geopersia* 14 (1): 89–111.
DOI: https://doi.org/10.22059/geope.2023.364334.648729.

Pankhurst M. J., Schaefer B. F., Turner S. P., Argles T., Wade C. E. (2013) The source of A-type magmas in two contrasting settings: U–Pb, Lu-Hf, and Re-Os isotopic constraints. *Chemical Geology* 351:175–194.
DOI: https://doi.org/10.1016/j.chemgeo.2013.05.010.

Pearce J. A. (1983) The role of sub-continental lithosphere in magma genesis at active continental margins. *Hawkesworth CJ, Norry MJ (editors.). Continental Basalts and Mantle Xenoliths. Shiva, United Kingdom: Nantwich*

Pearce J. A., Harris B. W., Tindle A. G. (1984) Trace element of discrimination diagrams for the tectonic interpretation of granitic rocks. *Journal of Petrology* 25:956–983.
DOI: https://doi.org/10.1093/petrology/25.4.956.

Plank T. (2005) Constraints from thorium/lanthanium on sediment recycling at subduction zones and the evolution of the continents. *Journal of Petrology* 46:921–944.
DOI: https://doi.org/10.1093/petrology/egi005.

Rapp R. P., Watson E. B. (1995) Dehydration melting of metabasalt at 8-32 kbar: implications for continental growth and crust-mantle recycling. *Journal of Petrology* 36:891–931.

Rollinson H. R. (1993) Using geochemical data: evaluation, presentation, interpretation. *Publishing House, Longman Group, United Kingdom*

Rudnick R. L., Gao S. (2003) Composition of the continental crust. *In Rudnick RL. 1nd ed. Treatise on Geochemistry, India: Elsevier,*
DOI: https://doi.org/10.1016/B0-08-043751-6/03016-4.

Sabzehei M. (1974) Les melanges ophiolitiques de la region d Esfandagheh (Iran meridional). Et ude petrographique et structurale. *PhD, University of Grenoble, France*

Salavati M., Kananian A., Nogheyan M. (2013) Geochemical characteristics of mafic and ultramafic plutonic rocks in southern Caspian Sea Ophiolite (Eastern Guilan). *Arabian Journal of Geosciences* 6:4851–4858. DOI: https://doi.org/10.1007/s12517-012-0688-1.

Salavati M., Kananian A., Noghreian M., Darvishzadeh A., Samadi Soofi A. (2008) Discovery of a Neo-Tethyan ophiolite in Northern Iran: Evidence for its formation at a slow-spreading center. *Journal of the Virtual Explorer* 28 (2)
DOI: https://doi.org/10.3809/jvirtex.2008.00188.

Salehpour S., Arian M. A., Jafari Rad A., Zarei Sahamieh R., Yazdi A. (2025) Geochemistry and technomagmatic environment of Eocene volcanic rocks in Yuzbashi Chay region, west of Qazvin (Iran). *Iranian Journal of Earth Sciences* 17 (1): 1–13.
DOI: https://doi.org/10.57647/j.ijes.2025.1701.04.

Schiano P., Monzier M., Eissen J. P. (2010) Simple mixing as the Major control of the evolution of volcanic suites in the Ecuadorian Andes. *Contributions to Mineralogy and Petrology* 160:297–312.

Shafaii Moghadam H., Li X. H., Ling X. X., Stern R. J., Zakikheder M., Chiaradia M., Ghorbani G., Arai S., Tamura A. (2015) Devonian to Permian evolution of the Paleo-Tethys Ocean: New evidence from U–Pb zircon dating and Sr-Nd–Pb isotopes of the Darrehanjir–Mashhad ophiolites, NE Iran. *Gondwana Research* 28:451–904.
DOI: https://doi.org/10.1016/j.gr.2014.06.009.

Shellnutt J. G., Jahn B. M., Zhou M. F. (2011) Crustally-derived granites in the Panzhihua region, SW China: Implications for felsic magmatism in the Emeishan large igneous province. *Lithos* 123:145–157.
DOI: https://doi.org/10.1016/j.lithos.2010.10.016.

Shellnutt J. G., Zhou M. F. (2007) Permian peralkaline, peraluminous and metaluminous A-type granites in the Panxi district, SW China: their relationship to the Emeishan mantle plume. *Chemical Geology* 243:286–316. DOI: https://doi.org/10.1016/j.chemgeo.2007.05.022.

Su Y. P., Zheng J. P., Griffing G. L., Zhao L. H., O´Reilly S. Y., Tang H. Y., Ping X. Q., Xiong Q. (2013) Petrogenesis and geochronology of Cretaceous adakitic, I- and A-type granitoids in the NE Yangtze block: constrants on the eastern subsurface boundary between the North and South China blocks. *Lithos* 175-176:333–50.

Sun S. S., McDonough W. F. (1989) Chemical and isotopic systematics of ocean basalts: Implications for mantle composition and processes. *Geological Society, London, Special Publications* 42:313–345.
DOI: https://doi.org/10.1144/GSL.SP.1989.042.01.19.

Turner S. P., Foden J. D., Morrison R. S. (1992) Derivation of some A-type magmas by fractionation of basaltic magma; an example from the Padthaway Ridge, South Australia. *Lithos* 28:151–179.
DOI: https://doi.org/10.1016/0024-4937(92)90029-X.

Valizadeh M. V., Abdollahi H. R., Sadeghian M. (2008) Geological investigations of main intrusions of Central Iran. *Geosciences Scientific Quarterly Journal* 17:182–197.
DOI: https://doi.org/10.22071/gsj.2009.57829.

Wang Y., Yang Y. Z., Siebel W., Zhang H., Zhang Y. S., Chen F. (2020) Geochemistry and tectonic significance of late Paleoproterozoic A-type granites along the Southern margin of the North China Craton. *Scientific Reports* 10:1–15.
DOI: https://doi.org/10.1038/s41598-019-56820-1.

Whalen J. B., Currie K. L., Chappell B. W. (1987) A-type granites: geochemical characteristics, discrimination and petrogenesis. *Contributions to Mineralogy and Petrology* 95:407–419.
DOI: https://doi.org/10.1007/BF00402202.

Whitney D. L., Evans B. W. (2010) Abbreviations for names of rock-forming minerals. *American Mineralogist* 95:185–187.
DOI: https://doi.org/10.2138/am.2010.3371.

Windley B. F., Xiao W. (2018) Ridge subduction and slab windows in the Central Asian Orogenic Belt: Tectonic implications for the evolution of an accretionary orogen. *Gondwana Research* 61:73–87.

Wu D. Q., Sun F. Y., Pan Z. C., Tian N. (2021) Geochronology, geochemistry, and Hf isotopic compositions of Triassic igneous rocks in the easternmost segment of the East Kunlun Orogenic Belt, NW China: Implications for magmatism and tectonic evolution. *International Geology Review* 63 (4): 1011–1029.
DOI: https://doi.org/10.1080/00206814.2020.1740895.

Wu F. Y., Sun D. Y., Li H. M., Jahn B. M., Wilde S. A. (2002) A-type granites in northeastern China: age and geochemical constraints on their petrogenesis. *Chemical Geology* 187:143–173. DOI: https://doi.org/10.1016/S0009-2541(02)00018-9.

Xiong X. L., Adam J., Green T. H. (2005) Rutile stability and rutile/melt HFSE partirioning during partial melting of hydrous basalt: implications for TTG genesis. *Chemical Geology* 218:339–59.

Xu C., Huang Z., Qi L., Fu P., Liu C., Li E., Guan T. (2007) Geochemistry of Cretaceous granites from Mianning in the Panxi region, Sichuan Province, southwestern China: Implications for their generation. *Journal of Asian Earth Sciences* 29:737–750. DOI: https://doi.org/10.1016/j.jseaes.2006.03.013.

Yajam S., Ghalamghash J. (2019) A-type granites of North Sanandaj-Sirjan zone, new observation, new classification. *journal of Geosciences* 29:221–320. DOI: https://doi.org/10.22071/gsj.2018.125685.1436.

Yang J. H., Wu F. Y., Chung S. L., Wilde S. A., Chu M. F. (2006) A hybrid origin for the Qianshan A-type granite, northeast China: geochemical and Sr-Nd–Hf isotopic evidence. *Lithos* 89:89–106. DOI: https://doi.org/10.1016/j.lithos.2005.10.002.

Yazdi A., Shahhosseini E., Moharami F. (2021) Petrology and tectono-magmatic environment of the volcanic rocks of West Torud–Iran. *Iranian Journal of Earth Sciences* 14 (1): 40–57. DOI: https://doi.org/10.30495/ijes.2022.1929200.1601.

Zaeimnia F., Kananian A., Salavati M. (2010) Petrogenesis of Southern Amlash alkaline rocks in the South Caspian Sea, North of Iran. *Journal of Geoscience* 20:69–78. DOI: https://doi.org/10.22071/gsj.2010.54599.

Zhang C. L., Zou H. B. (2013) Permian A-type granites in Tarim and western part of Central Asian Orogenic Belt (CAOB): Genetically related to a common Permian mantle plume? *Lithos* 172–173:47–60. DOI: https://doi.org/10.1016/j.lithos.2013.04.001.

Zhang H. F., Parrish R., Zhang L., Xu W. C., Yuan H. L., Gao S., Crowley Q. G. (2007) A-type granite and adakitic magmatism association in Songpan–Garze fold belt, eastern Tibetan Plateau: Implication for lithospheric delamination. *Lithos* 97:323–335. DOI: https://doi.org/10.1016/j.lithos.2007.01.002.

Zhang K. J. (2014) Genesis of the Late Mesozoic Great Xing'an Range Large Igneous Province in eastern central Asia: A Mongol–Okhotsk slab window model. *International Geology Review* 56:1557–1583.

Zhu L., Zhang G., Guo B., Lee B., Wang F. (2010) Geochemistry of the Jinduicheng Mo- bearing porphyry and deposit, and its implications for the geodynamic setting in East Qinling, P. R. China. *Chemie der Erde Geochemistry* 70:159–174. DOI: https://doi.org/10.1016/j.chemer.2009.12.003.